Compliant Gripping Mechanism for Anchoring and Mobility in Microgravity and Extreme Terrain

Undergraduate Honors Thesis

Submitted to the Department of Mechanical Engineering

The Ohio State University

In Partial Fulfillment of the Requirements

For Graduation with Honors Distinction in Mechanical Engineering

by

Collin Everett Mikol

May 2017

Defense Committee:

Dr. Haijun Su, Advisor

Dr. Ryan Harne

Abstract

One major limitation of previous NASA missions in exploring asteroids, comets, and planetary surfaces such as Mars has been the inability to properly navigate these terrains with conventional mobility methods. For example, the Mars Exploration Rover (MER), Opportunity, viewed stratified bedrock in a crater wall of Mars but was unable to access the samples due to its limited mobility. Traditional land rovers cannot maneuver well in extreme space environments with microgravity conditions because of the harsh terrain and very low escape velocities on smaller bodies. Land rovers are also incapable of traversing steep crater walls and cliffs, which limits the rover's ability to reach sites of greater scientific interest. Current drawbacks of space mobility technology lead to the opportunity to develop new, unique robots that have the ability for vertical climbing and locomotion in microgravity environments. This research focuses on developing a new technology that utilizes an array of small microspine grippers to provide the required forces to latch onto various types of rock formations. These grippers would increase a robot's ability to effectively travel in a microgravity environment and would allow rovers to climb vertical rock faces efficiently. The research objectives will be to develop, prototype, test and optimize a new concept design for a compliant mechanism microspine gripper to achieve higher load sharing capabilities with the constraints of minimizing the overall area and stresses created within the design itself. Quick design prototypes will be iteratively manufactured and tested to check for feasibility, and a final design will be optimized through the use of linear and non-linear beam bending equations. The higher load sharing capabilities of the design will ensure that the microspines will not fail to grasp rock in critical NASA missions. A unique geometry compliant mechanism design would achieve these goals. This could ultimately lead to climbing

robots that would possess a greater capability of harsh terrain and microgravity exploration with increased reliability.

Acknowledgements

I would like to say a big thank you to my research advisor, Dr. Haijun Su. Dr. Su played a significant role in the success and advancement of this project through his continual support and guidance. He was always very patient with me and willing to sit down and answer any nagging questions I had. His constant encouragement and motivation developed me as a better researcher, continuously pushing me to my limits to help me achieve my goals. For that I am very grateful.

I would also like to thank all of the other graduate students in the Design Innovation and Simulation Lab. Starting out in research was a daunting and scary task for me, but everyone in the lab was compassionate and willing to share their expertise with me from the very beginning of my research experience all the way through to completion. They helped me learn how to use all the various equipment in the lab and also supported me with any difficulties I had.

I also owe a big thank you to Dr. Robert Siston for the overall guidance and support in the Honors Undergraduate Research class. Dr. Siston's critiques of research presentations and abstracts have also helped me greatly develop as both a person and a researcher.

Finally, I would like to thank my amazing parents, Dale and Daria Mikol, for fully supporting me in pursuing research and a graduate degree. Their love and support throughout this whole process has been monumental in keeping me focused and motivated to achieve my goals. Without them, none of this would have been possible.

Table of Contents

List of Figures

List of Tables

Chapter 1: Introduction

Increased interest has been placed on exploring asteroids, comets, and other planetary surfaces as a stepping stone for future Mars missions, as evidenced by recent missions such as DAWN, Deep Impact, NEAR, and Hayabusa (Parness, 2011). Robotic analysis of these bodies is an essential first step in making future missions safe for humans. To date, only a few forms of mobility methods have successfully been utilized on space explorations, while others have been launched but failed to reach their destinations (Anon., 2015). Current mobility methods must be matured in order to successfully maneuver on and anchor to these terrestrial surfaces. This research paper focuses primarily on one of those methods, a microspine gripping mechanism that can be incorporated into a robot for vertical climbing and anchoring to surfaces in a microgravity environment.

1.1 Microspine Background

Microspines were originally invented at Stanford University in 2004 and have since been developed and shown to have working capabilities incorporated on climbing robots, in the landing gear of unmanned air vehicles, and in human climbing paddles (Parness, et al., 2013). Figure 1 shows one of the original concepts for the microspine design which consisted of both elastic flexures and a rigid frame with a large embedded steel hook mounted at the end. These microspines were arrayed into carriages that can contain anywhere from ten to one hundred microspines which can share and distribute the load between many attachment points. An example of a different microspine design arrayed in carriages is shown in Figure 2.

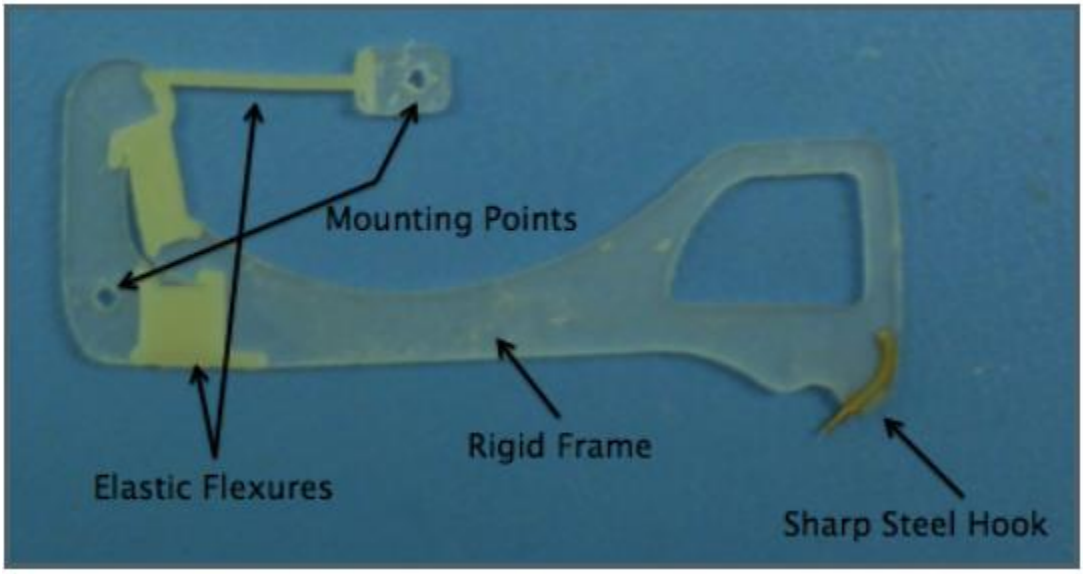

Figure 1: Original Microspine Concept

Figure 2: Microspines Arrayed into Multiple Carriages

As seen in Figure 2, each microspine has its own suspension structure which allows the microspines to drag independently of one another so each spine can grasp onto a different surface niche. This property allows the robot to support high loads during climbing or anchoring, as forces are uniformly distributed across different microspines within the array. Another

important property of microspine anchors is that they do not require any preload force to engage, only requiring brief surface contact (Parness, et al., 2012). This asset is beneficial to the proposed use in space-related applications because having no preload reduces the chances of failure and could help in reducing the stresses within the mechanism. Only requiring brief surface contact could also help with establishing a strong, secure first anchor with the rock surface.

1.2 Bio-Inspiration

There have been many different methods of adhesion tested and employed on climbing robots in recent years that mimic animals found in nature. Approaches such as suction cups, magnets, and sticky adhesives have been used to climb smoother vertical surfaces such as windows; however, these technologies are not suitable for use on hard, dusty exterior surfaces such as stone or rock (Kim, et al., 2005). Animals that exhibit scansorial (vertical surface) agility utilize a variety of different methods for vertical climbing. Geckos employ a very large number of fine hairs that use Van Der Waals forces for climbing (Autumn, et al., 2005). Larger animals such as cats use large, sharp claws that are able to penetrate softer surfaces such as wood. Smaller insects and arthropods utilize small, sharp spines that are able to latch onto fine surface indentations. This microspine technology research will focus on the latter method, utilizing small sharp spines to latch onto microscale surface asperities to use for vertical climbing.

What is unique about these spines as opposed to other researched methods for vertical robotic climbing is that the spines don't need to penetrate the rock surface; they merely grasp onto the small surface asperities, and the many microspine toes provide the required forces for the robot to climb. This concept is illustrated in Figures 3 and 4, which show a spine engaging a

concrete profile and the interaction between a microspine and surface asperities, respectively. It should also be noted that the microspines are capable of attaching to either concave or convex surface roughness. A dry microspine technology is also more attractive for climbing hard, dusty exterior surfaces as opposed to a "wet" adhesive like geckos use because the primary application for this technology will be used in extreme space environments.

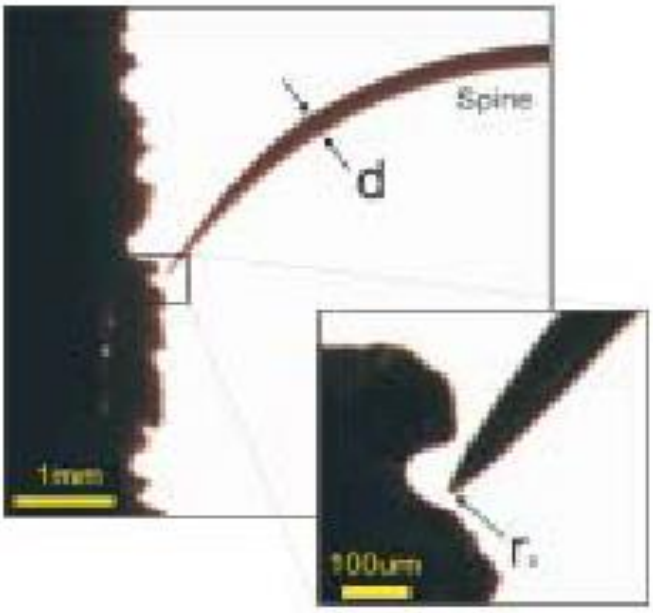

Figure 3: Spine Engaging a Concrete Profile

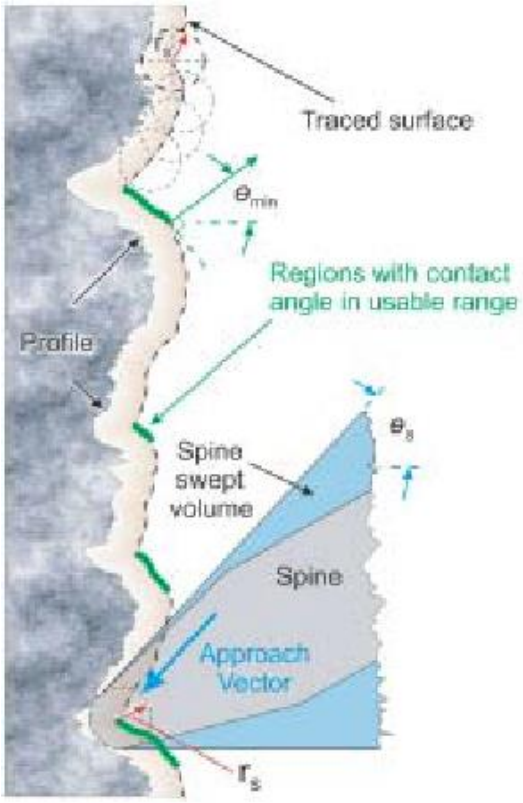

Figure 4: Microspine/Surface Interaction

1.3 Motivation

There are many potential applications for further developing this microspine technology, having both space-related and near-Earth scientific benefits. One obvious use is implementing microspines into rovers for operation in the extreme terrain conditions of Mars. Another possible implementation is using microspines as an anchoring mechanism to support drilling forces in the

microgravity environment of an asteroid in order to obtain scientific data samples. Further near-Earth uses could be to explore canyons or cliffs, or for use in metropolitan environments to climb the sides of high-rise buildings. Additional information into some possible scenarios where microspines could be beneficially used are detailed below.

1.3.1 Mars Exploration

As mentioned previously, some of the current rovers used in Mars exploration missions such as the Mars Exploration Rover (MER) have been limited by their mobility, only being able to traverse flat ground or slopes of less than 25 degrees. However, previous rover missions have spotted valuable scientific targets such as stratigraphy of exposed rock formations on faces of cliffs and lava tubes that are inaccessible to current rover designs (Parness, 2011). Geologic examination of the subsurfaces of these rock formations could increase scientific understanding of the formation and history of a planet or moon, and also increase our knowledge of the Solar System as a whole (Zacny, et al., 2008). Martian caves, lava tubes, and the planet subsurface are also more interesting areas for scientific study because they are protected against heavy doses of radiation, wind, and ultraviolet light, making them more hospitable in the search for life on Mars (Parness, et al., 2013). Although these areas are currently inaccessible, further research into the design of compliant mechanism microspines could make acquiring data samples from these locations possible in the near future.

1.3.2 Exploration of a Near-Earth Asteroid

Although some bigger asteroids have large and sufficiently strong gravitational fields for conventional mobility methods (i.e. a traditional land rover) to be adequate, smaller asteroids lack the necessary gravitational force for these wheeled robots to work effectively. In some

cases, depending on the size of the asteroid, the escape velocity for a rover can be smaller than 10 cm/second, rendering conventional travel methods virtually useless (Parness, 2011). Microspine technology, however, would allow rovers to quickly and safely anchor to the surface of an asteroid and provide an alternate means of locomotion across the surface.

Another situation involved with the exploration of near-earth asteroids is percussive drilling into the asteroid surface. The goals of these drilling operations are obtaining samples for in situ analysis, obtaining data samples for geology, geochemistry, and geophysics objectives, and providing an access hole for measurement tools to check for the presence of water (Zacny, et al., 2008). If the rover is scouting for a future manned mission to the asteroid, another reason for drilling is to install a network of support cables to increase the mission safety of the astronauts. This initial setup will allow more time for exploration by the astronauts (Parness, et al., 2013). Traditional land rovers would not be able to support the forces caused by drilling into the asteroid, but the anchoring ability of a rover incorporated with microspines would be able to counteract the necessary preload force, allowing drilling to be a viable operation.

1.3.3 Asteroid Trajectory Alteration

Near-Earth Asteroids and Comets pose two unique but very different scenarios: they can be used as an opportunity for greater scientific research and testing while also posing a threat to collide with Earth, triggering excessive loss of life or possibly human extinction. In order to address these situations, NASA's Asteroid Redirect Mission (ARM) focuses on the possibility of capturing a multi-ton boulder to place in the moon's orbit to alter the trajectory of the asteroid (Abell, et al., 2016). However, technologies to alter the trajectory of an object are still immature (Parness, et al., 2013). Microspine technology could be one possible solution to undertaking this challenge, ranging from utilizing its enhanced microgravity mobility to place thrusters or

explosives, or use its gripping capabilities on a larger scale to pick up a boulder from the asteroid.

1.4 Previous Research

Although there has been relative success with some of the previous microspine designs shown in Figure 5, there any many pending problems with current designs, with one of the major ones being reliability. Typically only about 10-20% of microspine toes in current designs are able to grip onto a surface, which can lead to the mechanism either not engaging or engaging with a very weak grip that is prone to failure (Parness, 2011). This failure mode is unacceptable in critical NASA missions where there might only be one chance at a successful operation. Another limitation of current designs is their non-compliance. Since the application for microspines will be used in extreme space environments, elastic members cannot be used because of their inability to operate at the limits of extreme temperature ranges, and metal members do not exhibit the same flexibility as elastic ones. This research will focus on developing a compliant mechanism microspine gripper to solve this compliance problem.

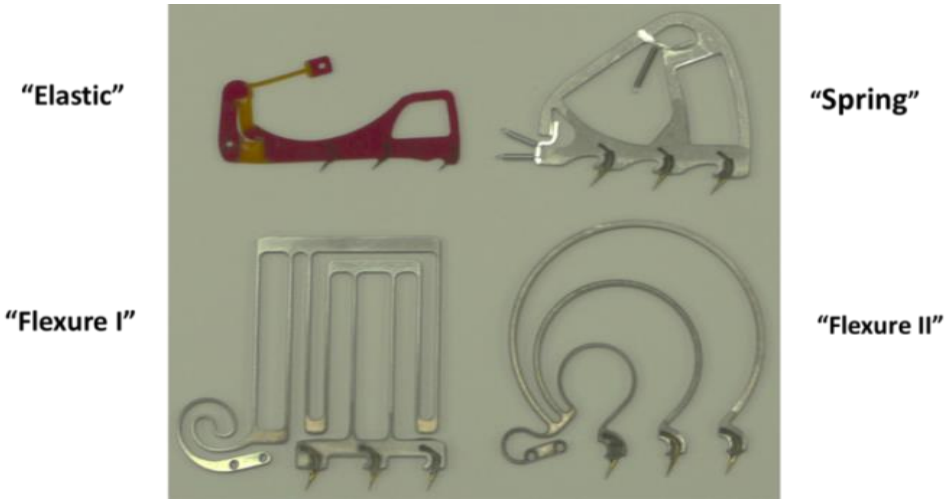

Figure 5: Examples of Previous Microspine Design Concepts

1.5 Focus of Thesis

The purpose of this research project was to develop a modified compliant mechanism microspine with decoupled spring stiffnesses having minimal size and higher load sharing capabilities than existing designs. Using my knowledge of kinematics, compliant mechanisms, and linear and curved beam analysis, I was able to design a monolithic compliant mechanism microspine with independent spring stiffnesses. This research also focused heavily on the design optimization of the beam models contained within the design, concentrating on minimizing both the stresses within the model and the beam lengths while increasing the loads they were able to support.

1.6 Significance of Research

Robotics and autonomous systems are continuously changing and paving the way for more advanced and safer space exploration. More specifically, a rover's mobility poses a critical capability for space exploration, as witnessed by nearly a decade and a half of recent planetary surface exploration (Anon., 2015). Space agencies such as NASA typically first deploy rovers in "scout" missions to planetary bodies that they want to explore (Parness, 2011). These missions are performed in order to determine the composition and physical properties of the planetary body in order to ensure the security of a future manned mission.

However, current space exploration rovers are limited by their ability to travel in extreme terrain environments on planetary bodies or in a microgravity environment of an asteroid. In extreme terrain environments, current land rovers are limited to travel on relatively flat ground with slopes no greater than 25 degrees. This poses the problem that the rover will not be able to explore lava tubes or crater walls which could contain scientifically important data samples

(Parness, 2011). In a microgravity environment on an asteroid, there is usually a lack of a normal force on the wheels, preventing the rover from moving. If there is a sufficient normal force, there is a high danger of the rover reaching the very low escape velocity and jettisoning off into space (Parness, et al., 2013). It is also extremely difficult to drill into an asteroid for rock samples with current rover designs because the rover cannot support the necessary pre-load force caused by the drilling.

By utilizing compliant mechanism microspines as a means for anchoring and mobility in these space exploration situations, we are able to offer a more reliable means to traverse cliffs and microgravity environments in any spatial orientation by having the microspines create strong and fast attachment to obscure rock formations. Microspines also offer higher flexibility, enhanced lateral movement and the ability to resist sampling forces much better than a typical land rover. A new design for a compliant microspine that has isolated stiffnesses parallel and perpendicular to the rock surface during operation will significantly increase the load carrying capacity each microspine can support while also creating greater adherance to the rock surface. These microspines can be arrayed into carriages to be used on climbing robots to provide a more versatile means of navigating in extreme terrain or microgravity environments.

1.7 Overview of Thesis

This thesis consists of 4 chapters. Chapter 1 provides a general overview of microspines with their applications, along with an overview of my thesis.

Chapter 2 includes the background of compliant mechanisms, discusses the design requirements for the microspines, and examines some of the materials considered for this application. This chapter also discusses some of the iterative processes used in order to develop a

fully functional compliant mechanism microspine gripper for use in extreme terrain or microgravity space environments. A discussion of the final design along with its functional capabilities is also provided.

Chapter 3 discusses an analysis and optimization of the design. This chapter provides an in-depth analysis into how a mathematical model of the design was created and then verified. This chapter also discusses how the microspine was improved to maximize the force to grasp rock while reducing the overall size of its beams to reduce the weight. It also includes calculations performed in Wolfram Mathematica in order to reduce the overall stresses within the design as well as Finite Element Simulation data to show important properties within the material.

Chapter 4, the conclusion, summarizes the key contributions of this thesis, discusses additional applications of this research, and proposes future directions of study.

Chapter 2: Microspine Design

2.1 Compliant Mechanism Background

One of the key requirements of this research project was to investigate compliant mechanism solutions to the design of the microspine gripper mechanism. Compliant mechanisms transfer or transform motion, force, or energy through an elastic deformation from flexible members rather than moveable joints only (Howell, 2001). One simple example of a compliant mechanism is a spring, which is able to store an initial displacement in the form of strain energy and then return elastically to its original position. Howell lists several major advantages to using compliant mechanisms as opposed to rigid-body mechanisms (Howell, 2001):

1. Dramatic reduction in the total number of parts required to accomplish a specified task, which may reduce manufacturing time and assembly cost and increase reliability.
2. Compliant mechanisms have fewer moveable joints which results in reduced wear and need for lubrication. These characteristics are especially valuable for operation in harsh environments that may adversely affect joints.
3. Fewer joints can lead to a complaint mechanism that has increased precision and a highly repeatable motion. This is due to the fact that backlash is significantly reduced or eliminated.
4. Vibration and noise are also reduced since the motion is achieved from deflection rather than by adjoining parts rubbing against one another.
5. Since energy is stored in the form of strain energy in the flexible members, the energy is easily stored or transformed to be released at a different time or in a different manner.

Compliant mechanisms also have a few disadvantages:

1. Since many of the flexible members undergo large deflections, linearized beam equations are no longer valid which makes analysis more difficult.
2. The motion from the deflection of compliant links is limited by the strength of the deflecting members.
3. Fatigue analysis is a vital consideration since compliant members are often loaded cyclically and must have sufficient fatigue life to perform their prescribed functions.

Although there are some minor disadvantages to using compliant mechanisms, the advantages listed above are highly suitable for compliant mechanism use in the development of a microspine gripper. The increased precision and highly repeatable motion suggests compliant

mechanism microspines will be very suitable for anchoring and vertical climbing in extreme space and microgravity conditions. The elimination of the need to apply lubrication to any joints or hinges is also a major advantage, reducing the need for microspine maintenance.

2.2 Design Requirements

The design requirements for this microspine were initially given to me, having been created from previous research experiments incorporating microspines into climbing and grasping robots. Optimal stiffness and travel distance values were found from previous elastic microspines. This research will focus on the design of a compliant microspine from a metal, non-elastic material to withstand harsh space environments. Table 1 below lists some of the key design requirements. The X direction is parallel to the surface to be gripped while the Z direction is orthogonal to the surface.

Table 1: Key Design Requirements for the Compliant Mechanism

Criterion	*Target Value*	*Reasoning*
Kx	0.5 N/mm	Strength to support high loads
Kz	0.005 N/mm	Self-adapting to rock surface
Delta x	12 mm	Increased likelihood of grasping rock
Delta z	10 mm	Reduces overall stress
Maximum Rotation	15°	Reduces overall stress
Microspine Area	75 mm x 75 mm x 2 mm	Reduced footprint and reduced weight
Minimum Factor of Safety	1.25	Increased reliability

The stiffness values in the x-direction and z-direction were important target values to achieve during the research project. The higher stiffness (0.5 N/mm) in the direction parallel to the surface allows the microspines to support larger loads when grasping rock surfaces, reducing

the probability of failure. A lower stiffness (0.005 N/mm) orthogonal to the surface helps the mechanism conform to the surface easier and makes it self-adapt to the surface as the microspine toes are dragged across it. The goals for the travel distances are also important in increasing the likelihood of finding a stable attachment point to the surface.

In addition to some of the quantitative design requirements listed in Table 1, further qualitative objectives were created for the design to meet. These objectives include:

- The mechanism is simple and can easily be manufactured from one piece of material
- The mechanism can nest with itself to allow for a greater microspine compactness
- The “x” and “z” displacements are independent from each other as much as possible

A simplified diagram of the design goal showing independent x and z displacements is shown in Figure 6. If the two joints in the diagram represent a simple prismatic or slider joint, it can be shown that the mechanism can move horizontally without affecting the vertical stiffness and can likewise move vertically without affecting the horizontal stiffness. It was important during the design process to try to isolate these stiffnesses as much as possible in order to achieve a higher horizontal stiffness for supporting high loads while having a lower vertical stiffness so the mechanism can conform more easily to the rock surface.

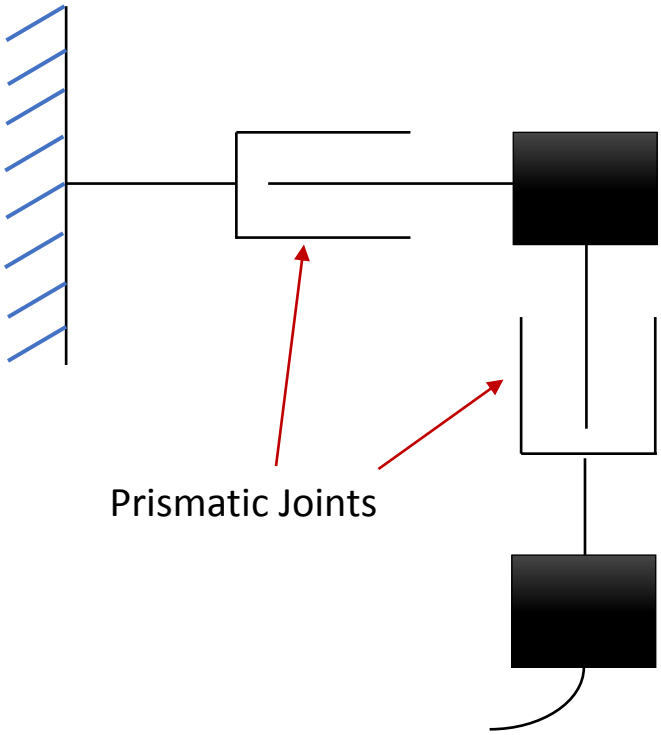

Figure 6: Simplified Diagram of Design Goal

2.3 Material Selection

The selection of an appropriate material for this design application is essential for multiple reasons. The selected metal must be flexible enough to deflect under a large load while still being very strong in supporting loads, must not be brittle or prone to fatigue failure, and must be suitable for harsh environmental conditions such as space, where this device is planned on being used. Before discussion of how an appropriate material was chosen for this research project, a few definitions will be made to alleviate some common misconceptions about properties of metallic alloys. Specifically, the relationship between a material's stiffness, strength, and flexibility will be reviewed.

Stiffness is a function of the material's properties such as its Young's Modulus and its geometry and boundary conditions. More specifically, it is the force divided by the deflection at a given point. Strength is a material property based on the Yield Strength of the material and is

the maximum stress that a material can withstand before plastic failure. More simply put, strength determines the maximum stress that can occur before failure while stiffness determines how much deflection will occur due to a specified load (Howell, 2001). Flexibility, also known as compliance, is the ability of a member to deflect under a load and is based upon material properties, geometry, and boundary conditions. While one does not want most rigid-body mechanisms to be flexible, high deflections are desirable to be achieved in compliant mechanisms with the smallest possible loads and member stresses. The conclusion from these definitions is that it is possible to make compliant members both flexible and strong. This is why material selection was a key part of the design process.

Table 2 shows a list of Young's Modulus, Yield Strength, and the ratio between the two for some common materials. A materials' compliance is directly related to its Yield Strength divided by its Modulus as shown in equation (1).

$$Compliance \ \alpha \ \frac{S_y}{E} \tag{1}$$

A larger ratio means the material can have a larger deflection before plastic failure. From the table, Aluminum 7075 and Titanium 13 heat treated were the two metals that exhibited the highest compliance levels, so they were the primary metals experimented with in this research. Non-metallic materials were excluded from evaluation because of their inability to operate properly in extreme temperature environments like space. Steel 4140 was also excluded from consideration because the material's properties were after quenching and tempering, thereby making the material less common than a general Aluminum or Titanium. After performing simple calculations to test deflections on some of the design ideas, it could be clearly seen that the Titanium material was the best option. The use of titanium reduced the overall size of the design while meeting stiffness criteria, a key design requirement for the project. Therefore,

Titanium 13 heat treated was selected as the optimal material to base all the design calculations on. All results from calculations shown in future sections will use Titanium as the mechanism material.

Table 2: Ratio of Yield Strength to Young's Modulus for Various Materials

Material	E (Gpa)	S_y	(S_y/E) *1000
Steel (1010 hot rolled)	207	179	0.87
Steel (4140 Q&T @ 400)	207	1641	7.9
Aluminum (1100 annealed)	71.7	34	0.48
Aluminum (7075 heat treated)	71.7	503	7
Titanium (Ti-35A annealed)	114	207	1.8
Titanium (Ti-13 heat treated)	114	1170	10
Nylon (type 66)	2.8	55	20
Kevlar (82 vol %) in epoxy	86	1517	18

2.4 Concept Ideation

Development of a new compliant mechanism microspine design involved using many principles of the design process. After the design requirements were established as discussed in section 2.2, preliminary design sketches were drawn and modeled from previous microspine designs to get an idea of how the design would look and function. Numerous design sketches were created from many inspirational ideas of mechanisms learned from previous classwork to help get a better idea of a model for a planar design of a compliant mechanism. Feasibility assessments and design matrices were also implemented for most of the concepts generated to see how well they would meet the design requirements specified by NASA JPL in Table 1 for this project.

For the initial design concepts, the motion in the vertical direction was constrained by slider joints while the motion parallel with the surface was determined by the deflections of a cantilever beam with the microspine hook at the end. This design orientation was chosen because required stiffness in the vertical direction was very small and hard to meet using conventional springs, whereas a slider joint has essentially zero stiffness. Four of the initial design prototypes are shown in Figure 7.

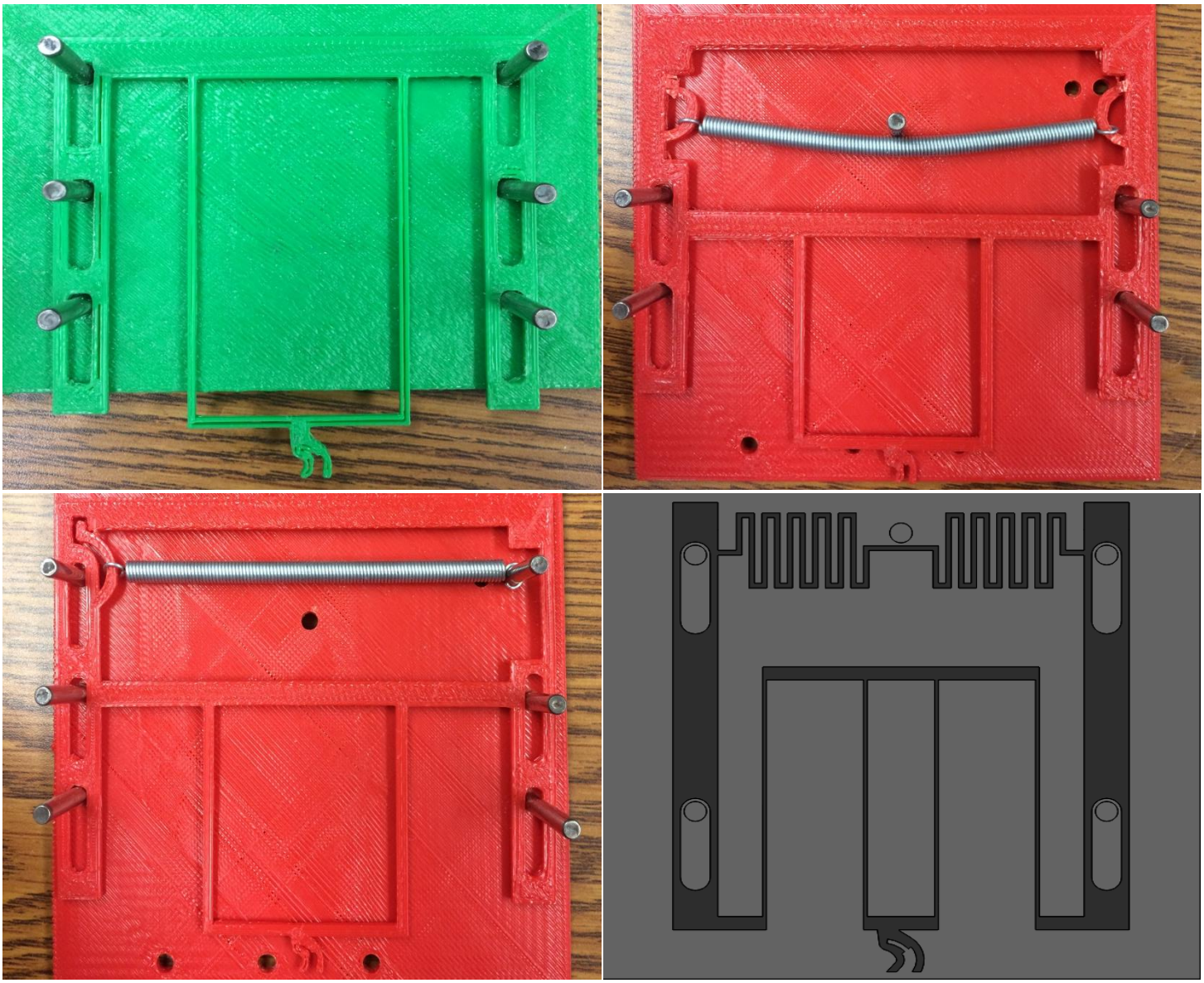

Figure 7: Initial Design Concepts

One of the first concept prototypes, shown in the upper left picture of Figure 7, utilizes slider joints for motion in the vertical direction and a cantilever beam with one end fixed and the other end guided for grasping rock in its horizontal motion. A main drawback of this design was that although it meets the requirements for less than 0.005 N/mm stiffness in the vertical direction, the stiffness is too low, being zero for a sliding joint. This renders the design impractical because of the reliance on gravity to bring the mechanism back to its starting position after the force on it has been released. In a microgravity environment like space, one cannot rely

on gravity alone to restore the mechanism back to its starting position. There needs to be a small restoring force that pushes the mechanism downwards and back into the rock surface to enable the mechanism to grip effectively.

Prototypes in the upper-right and lower-left of Figure 7 were developed to use a 3D extension spring to provide a restoring force to keep the mechanism in contact with the surface. The issues with these designs, however, were that for the upper-right design, the vertical stiffness was too high and the horizontal stiffness was also very stiff. In the lower-left design, the extension spring was attached to the mechanism at one end and to a fixed stationary pin at the other end. This served to greatly reduce the vertical stiffness. However, the problem with the design was that it was no longer symmetric. The mechanism had a tendency to rotate and jam very easily when a vertical force was applied. An analysis was also performed on the vertical beams, modeling them as one end fixed and the other end guided. The maximum deflection for this beam type is shown from Equation (2). Solving for the stiffness value of two connected cantilever beams, the k_x stiffness for this beam type is calculated from Equation (3).

$$y_{max} = \frac{FL^3}{12EI} \tag{2}$$

$$k_x = \frac{24EI}{L^3} \tag{3}$$

Equation (3) was used to solve for the length of the cantilever beam using Titanium-13 as the material, a uniform thickness of 0.5 mm, and out-of-plane thickness of 1.5875 mm. In order to meet the required stiffness value of 0.5 N/mm, the required length was found to be 44.89 mm. In an attempt to reduce this vertical length further, the design concept in the lower-right of Figure 7 was analyzed using a double parallelogram beam design. This design also implemented a 2D planar spring, shown in Figure 8, to introduce a very small stiffness for the vertical mechanism motion. Figure 8 shows a diagram of half of the spring with listed design parameters. A full optimization was performed on the spring but the vertical spring segments were found to be too long and out of range of the design goal from Table 1. The full optimization code with results can be seen in Appendix A.

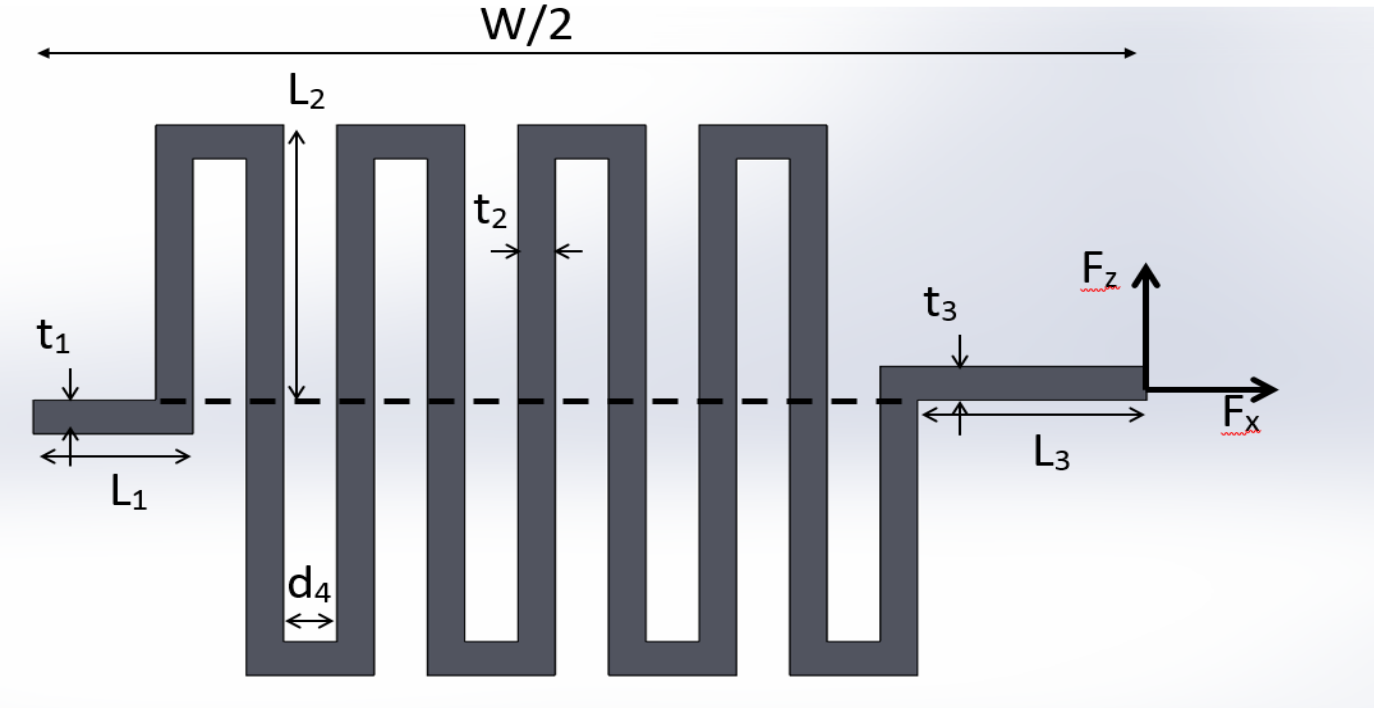

Figure 8: Half Spring Diagram with Design Parameters

2.5 Final Design

The final concept design that was created was made by combining all of the positive aspects of the prototypes that meet the design goals required in Table 1 and eliminating all of the negative design aspects. The final microspine mechanism design is shown below in Figure 9 and will be analyzed in future sections of this research paper.

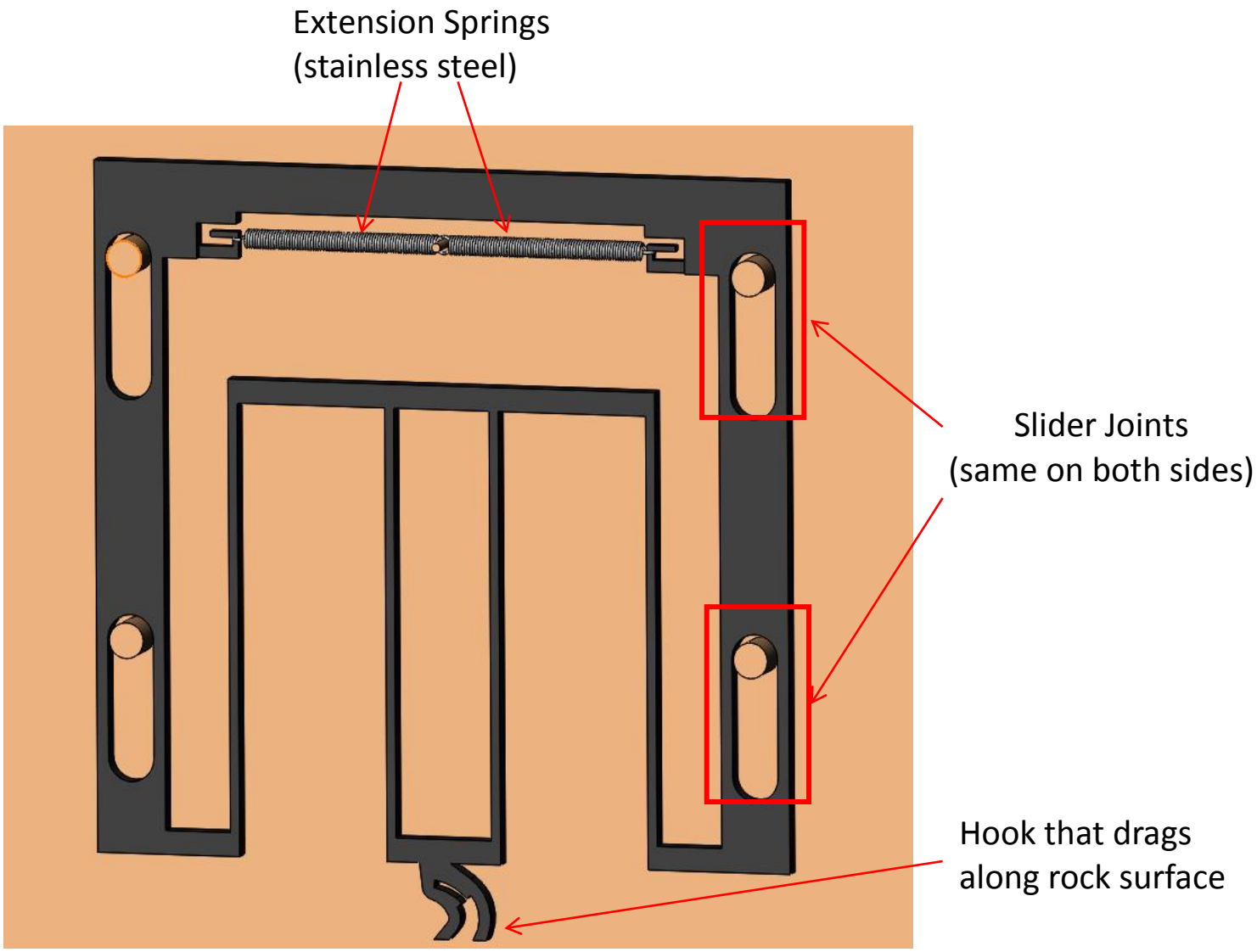

Figure 9: Final Microspine Mechanism Design

As can be seen in Figure 9, the horizontal motion of the mechanism is achieved from the double parallelogram cantilever beams with the hook at the end that drags along the rock surface.

When a vertical force is applied at the bottom of the spine, the motion in the vertical direction is constrained by the length of the slots for the slider joints. The stainless steel extension springs offer a restoring force to push the mechanism back down to its equilibrium position after it has been displaced upwards. These springs allow the mechanism to achieve the very low stiffness value of 0.005 N/mm in the vertical direction.

Another important aspect of the final design is that the stiffness values in the horizontal (k_x) and vertical (k_z) directions remain highly independent from one another, meaning motion in either direction will not affect the stiffness value in the other direction. By design, the Δx and Δz values are also constrained to 12mm and 10mm, respectively. The shape of the design limits these values, with the distance between vertical segments of the double parallelogram design constraining Δx and the lengths of the vertical slots constraining Δz. The overall rotation of the mechanism as a whole is also reduced due to it being constrained by the vertical slots, along with the double parallelogram beams that support the main loads to be fixed-guided beams, meaning their rotation at the end is zero degrees. A list of the overall design parameters for the final design is shown in Table 3. Appendix B shows the final design with a more in-depth diagram of the final design parameters that were chosen after the optimization.

Table 3: Final Design Length Values

Paramter	Value (mm)
Width	60.54
Height	60.98
Extension spring length	19.049
Slot Length	10

Chapter 3: Design Analysis and Optimization

Throughout the prototype and design process, various mechanism designs were analyzed to see how well the design requirements listed in Table 1 could be met. An analysis was performed on each prototype design to quantify the stiffness and deflection elements of the mechanism to see if it would be a plausible solution to the design challenge. In this chapter, an analysis and an optimization will be performed for the horizontal and vertical stiffnesses in order to reduce the overall size of the mechanism as well as increase its load sharing capabilities. It was important to do an analysis of the design before an optimization was performed to ensure that the derived equations closely matched the model and that it was possible to achieve the desired stiffness values with the chosen shape geometry.

3.1 Horizontal Stiffness (k_x) Design Analysis

The double parallelogram design in Figure 10 was analyzed to achieve the required stiffness value of 0.5 N/mm in the horizontal direction parallel with a surface.

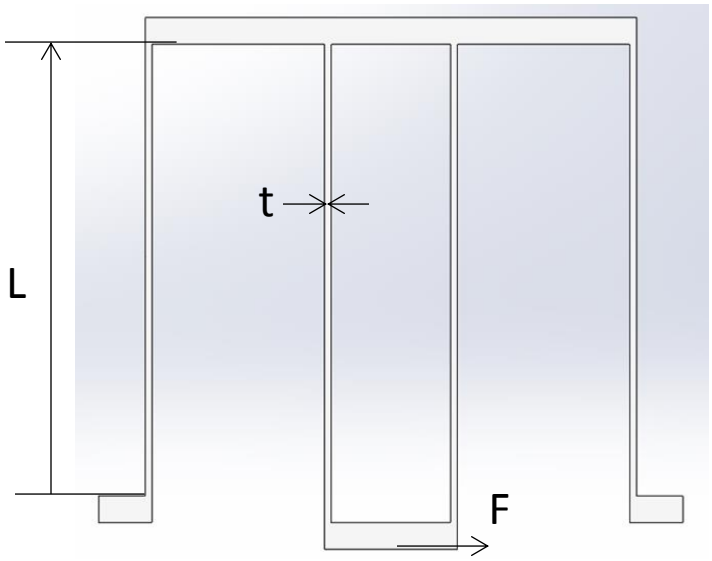

Figure 10: Double Parallelogram Beam Analysis

The beam model was based upon the beam with one end fixed and the other end guided model. The general solutions to this beam model are shown in equations (4) and (5).

$$y_{max} = \frac{FL^3}{12EI} \tag{4}$$

$$M_{max} = M_o = \frac{FL}{2} \tag{5}$$

To solve for the maximum stress within the model, equation (4) was solved for the force F and substituted into equation (5) to give equation (6).

$$M_{max} = \frac{6EIy_{max}}{L^2} \tag{6}$$

The general equation for maximum stress in a beam segment can be found from equation (7), where c is the thickness/2.

$$\sigma_{max} = \frac{M_{max}c}{I} \tag{7}$$

Substituting equation (6) into equation (7) and solving, the maximum stress in the beam is:

$$\sigma_{max} = \frac{3Et_{max}y_{max}}{L^2} \tag{8}$$

In order to calculate the deflection of the beam tip, Castigliano's Theorem can be used to find the internal strain energy within the beam and integrate over the length of the beam to find the total deflection. The internal strain energy is calculated from equation (9) as:

$$U_i = \int \frac{M^2}{2EI}\,dx \tag{9}$$

In this equation, however, both M and I are functions of x. Equation (9) can then be redefined for half of a beam segment as:

$$U_i = \int_0^{\frac{L}{2}} \frac{M(x)^2}{2EI(x)} dx \tag{10}$$

Since the moment M is defined as M=F*x, the partial derivative of this equation can then be taken with respect to the force F to find the deflection of the beam. This is shown in equation (11)

$$\Delta = \frac{\partial U_i}{\partial F} = \int_0^{\frac{L}{2}} \frac{M(x)}{EI(x)} * \frac{\partial M}{\partial F} * dx \tag{11}$$

Simplifying this equation, the overall end-tip deflection of a beam with length L/2 can be found from equation (12) (assuming a rectangular cross-section).

$$\Delta = \int_0^{\frac{L}{2}} \frac{Fx^2}{EI(x)} dx = \int_0^{\frac{L}{2}} \frac{12Fx^2}{bEt(x)^3} \tag{12}$$

Since equation (12) determines the deflection of only a half-beam segment, the overall deflection of the mechanism where the force is applied is found by multiplying this result by four. In order to test the validity of this model, the output deflection (Δ) for a given input force (F) needs to be determined assuming a constant thickness function for the beam thickness. The model parameters used to validate the code are given in Table 4. Once the parameters were defined, Wolfram Mathematica was used to solve the deflection based on equation (12). A SolidWorks model of the design was then created with the parameters from Table 4. A sensor was used to find the deflection of the spine tip to compare to the output of the Mathematica code.

Table 4: Model Validation Chosen Parameters

Variable	Definition	Assigned Value
F	Force applied to half-beam segment	0.5 N
b	out-of-plane thickness	1.5875 mm
t(x)	thickness of beam	0.5 mm
E	Young's Modulus for Titanium	1.14*10^5 N/mm
S_y	Yield Strength for Titanium	1170 MPa
L	Beam length	38 mm

Using the parameters listed in Table 4, the overall spine tip deflection was calculated using both equation (12) and results from the SolidWorks Model. It was found using equation (12) that the horizontal deflection of the mechanism was 1.21 mm while the SolidWorks model predicted a deflection of 1.27 mm. These values indicate a high correlation between the derived model for analysis and the SolidWorks model. One would expect the values to be slightly different because equation (12) uses small deflection theory while the SolidWorks model is using a non-linear solver to solve for large deflections.

3.2 Horizontal Stiffness (k_x) Design Optimization

After performing an analysis and verifying the accuracy of the beam models in the previous section, the next step was to optimize the design. The ultimate goal of the optimization was to find the thickness function t(x) of the beams to decrease the length (L) of the beams. This would minimize the overall size constraint while still having the mechanism retain all of its previous properties, including a 12mm travel distance, attaining the required stiffness value of 0.5 N/mm, and limiting the overall stress within the mechanism. Optimizations were performed

both in Wolfram Mathematica and with a SolidWorks Design Study. Results are shown in the upcoming sections.

3.2.1 Wolfram Mathematica Optimization

The double parallelogram model shown in Figure 10 was analyzed using the continuous beam model depicted in Figure 11.

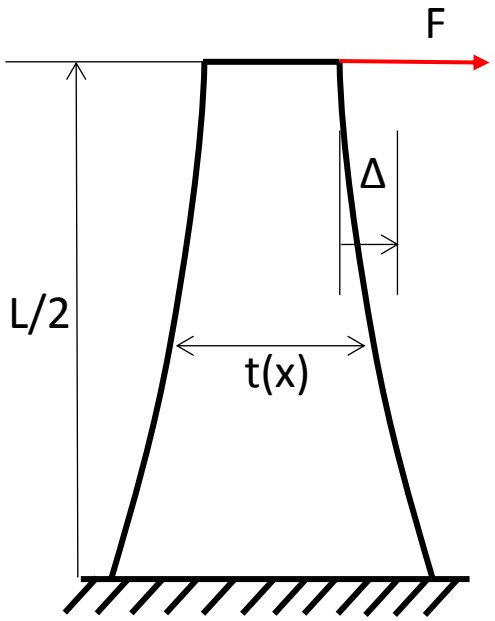

Figure 11: Continuous Beam Model

However, since we are now trying to find the thickness function that reduces the beam length and it is unknown, it is inconvenient to calculate the integration in equation (12) because the thickness will vary as a function of x. Therefore, a discretized model is needed which breaks up the beam into very small segments along its length to make the calculations easier. The discretized beam model is shown in Figure 12. This discretized beam model is different from the continuous model in that the beam is broken up into n different segments, each with a thickness of t_i so that the overall deflection can still be calculated.

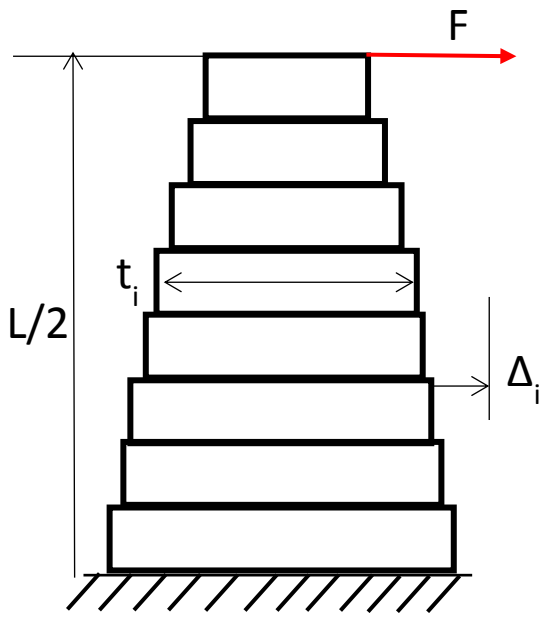

Figure 12: Discretized Beam Model

Using this discretized model, the deflection at each segment can be calculated as:

$$d(x_i) = \frac{12Fx^2}{bEt(x_i)^3} \tag{13}$$

The number of discretized segments and the x location of each deflection can be found from equations (14) and (15).

$$n = \frac{L/2}{\Delta x} \tag{14}$$

$$x_i = i\left(\frac{L/2}{n}\right) \tag{15}$$

Instead of using an integration as in equation (12), a summation is performed to find the deflection of the beam end-tip.

$$\Delta = d(x_i)\Delta x = \sum_{i=1}^{n} A_i = \sum_{i=1}^{n}\left(\frac{L/2}{n}\right) * \frac{12Fx_i^2}{bEt_i^3} \tag{16}$$

Also, since we know the required stiffness value k is 0.5 N/mm and F=kΔx, the force can be eliminated from equation (16) to get equation (17).

$$k_x = \frac{1}{\sum_{i=1}^{n}\left(\frac{L/2}{n}\right) * \frac{12x_i^2}{bEt_i^3}} \tag{17}$$

Substituting equation (15) into equation (17), it was then possible to reduce the equation further to get the result shown in equation (18).

$$k_x = \frac{1}{\left(\frac{L/2}{n}\right) * \frac{12}{bE} * \sum_{i=1}^{n}\frac{i^2}{t_i^3}} \tag{18}$$

Equation (18) could then be solved for the objective function of the length of the beam as a function of the thickness t_i and stiffness k_x. The simplified equation is shown as equation (19).

$$L = \sqrt[3]{\frac{2 * n^3 * b * E}{3 * k_x * \sum_{i=1}^{n}\frac{i^2}{t_i^3}}} \tag{19}$$

After defining the objective function for the length L in terms of the thickness, it was then necessary to define some of the constraints on the equation. These constraints are:

- Minimum beam thickness is ≥ 0.375 mm
- K_x=0.5 N/mm
- Max Stress ≤ (Yield Strength/Factor of Safety)

Using Wolfram Mathematica's FindMinimum command, an equation was set up to find the minimum value of the beam length and return the thickness function while also meeting the design constraints. The results from this optimization showed that the optimized beam length

was 30.9 mm. For the beam thickness, the result was a nearly uniform thickness beam at 0.436 mm. Full results of the Mathematica code are in Appendix A.

3.2.2 SolidWorks Optimization and FEA Results

Similar to the Mathematica optimization shown in subsection 3.2.1, a SolidWorks Design Study was also used as a tool to model the design and optimize the parameters of the beam segments to minimize the overall length of the vertical beam segments. The design was initially created with an overall vertical beam length of 40 mm with a constant thickness of 0.5 mm. Fewer parameters were defined in SolidWorks to make the optimization run faster; half of the beam was modeled and dimensioned and then mirrored. This ensured the beam was symmetric about the center and required defining fewer parameters in the study. In the Finite Element Analysis for the design study, the model was fixed at the bottom of the outside beams and the force applied in the center where the spine would be, as shown in Figure 13.

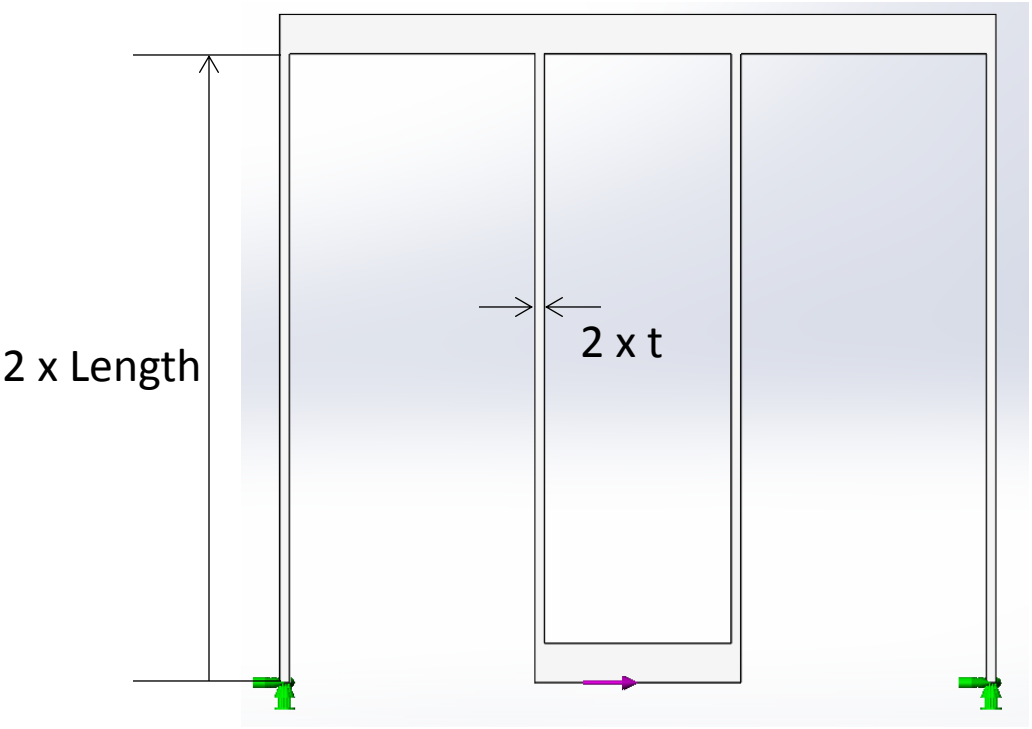

Figure 13: FEA Model with Fixed Beams and Applied Force

The variables defined for this optimization were half the beam thickness at six equally spaced locations along the length of the beam and the length of half of the vertical beam segment. These are shown in Table 5. The minimum value chosen was 0.1875 mm, since this is half of the smallest thickness of 0.375 mm which was chosen as the minimum for fabrication purposes.

Table 5: Variables used for Varying Thickness Optimization

t1	Range	Min:	0.1875mm	Max:	0.3mm		
t2	Range	Min:	0.1875mm	Max:	0.3mm		
t3	Range	Min:	0.1875mm	Max:	0.3mm		
t4	Range	Min:	0.1875mm	Max:	0.3mm		
t5	Range	Min:	0.1875mm	Max:	0.3mm		
t6	Range	Min:	0.1875mm	Max:	0.3mm		
Length	Range with Step	Min:	14mm	Max:	20mm	Step:	0.1mm

After setting all the parameters for the optimization, it was then necessary to define all of the constraints for the model. Two FEA Models were used to help characterize the stiffness values and displacements of the mechanism. The first analysis, named “Small Displacement” used an applied force of 0.1 N while the second analysis, named “Large Displacement”, used an applied force of 5.7 N. The small displacement analysis was used to validate the mechanism had a stiffness value of 0.5 N/mm at very low deflections. The large displacement analysis ensured that the mechanism was able to flex around 12 mm and that it could support a much larger load at this deflection. The large analysis was also used to calculate the maximum stress in the model and determine the factor of safety, ensuring both met the design goal requirements. The constraints Displacement2 and Displacement 3 in the table model the overall horizontal deflection of the mechanism. The constraints for this design study are shown in Table 6.

Table 6: Constraints used for Varying Thickness Optimization

Stress1	is less than	Max:	936 N/mm^2	Large Displaceme		
Minimum Factor of Safety1	is greater than	Min:	1.250000	Large Displaceme		
Displacement2	is between	Min:	0.18mm	Max:	0.22mm	Small Displaceme
Displacement3	is greater than	Min:	11.5mm	Large Displaceme		

With all of the variables and constraints for the model now defined, the SolidWorks optimization was run, analyzing each possible model and picking the optimal solution that meets all the design constraints. Table 7 contains the optimal values for the different variables chosen for this design study.

Table 7: Results for Varying Thickness Beams

Parameter	Value	Units
Overall Length	32	mm
Thickness Location 1	0.6	mm
Thickness Location 2	0.6	mm
Thickness Location 3	0.4875	mm
Thickness Location 4	0.375	mm
Thickness Location 5	0.4875	mm
Thickness Location 6	0.4875	mm
Max Stress	906.3	N/mm^2
Minimum Factor of Safety	1.29	-
Max Horizontal Displacement	11.51	mm
Supported Load	5.7	N

The results in Table 7 show the thickness of the vertical beams has a small variation between the six different segments. Since this design will eventually be manufactured by either Waterjet cutting or EDM cutting, this limits the precision of the dimensions one can attain on the beams. Therefore, another optimization was run in SolidWorks, this time using a uniform

thickness beam instead of trying to vary the thickness along the beams. Figure 13 shows the same starting model that was used for this optimization. This time however, a constant thickness for all the beams was modeled and the parameters are shown in Table 8.

Table 8: Variables used for Constant Thickness Optimization

Length	Range with Step	Min:	14mm	Max:	18mm	Step:	0.1mm
t1	Range with Step	Min:	0.19mm	Max:	0.3mm	Step:	0.01mm

Similar to constraints chosen for the varying thickness optimization shown in Table 6, a similar procedure was used for the uniform thickness optimization. The same constraints on stress and factor of safety were used. A 0.1 N force was again applied to the FEA analysis named "Small Displacement" but a 6 N force was applied to the analysis "Large Displacement" to try to support a larger load. The displacement range for the small displacement FEA analysis was also increased to span from 0.17 mm to 0.23 mm to increases the chances of a successful optimization. Displacement3 models the overall horizontal deflection and was increased to 11.9 mm to ensure the mechanism could travel 12 mm overall. The constraints used for this model are in Table 9.

Table 9: Constraints used for Uniform Thickness Optimization

Stress1	is less than	Max:	936 N/mm^2	Large Displaceme		
Minimum Factor of Safety1	is greater than	Min:	1.250000	Large Displaceme		
Displacement2	is between	Min:	0.17mm	Max:	0.23mm	Small Displaceme
Displacement3	is greater than	Min:	11.9mm	Large Displaceme		

The simulation was run and the results of the overall simulation are shown in Table 10. Since the dimensions for the length and thickness are halved in the model, the overall sizing of

the mechanism will have a length of 32.6 mm and thickness of 0.46 mm. These are the dimensions that were used for the final design shown in Figure 9.

Table 10: Final Results for Uniform Thickness

Parameter	Value	Units
Length	16.3	mm
t1	0.23	mm
Stress1	933.4	N/mm^2
Minimum Factor of Safety	1.253	-
Displacement2	0.206	mm
Displacement3	12.056	mm

From Table 10, it is seen that at a 0.1 N force the displacement of the mechanism is 0.206 mm. This gives a stiffness value of approximately 0.49 N/mm at a small deflection which was the required k_x stiffness goal. The large displacement analysis shows that each microspine mechanism can theoretically support up to 6 N before failure and flexes up to 12.056 mm, meeting the design goal.

Using the results from Table 10, an FEA Analysis was run in SolidWorks to confirm the properties of the mechanism. Figures 14 and 15 show the stress distribution within the model and the factor of safety plot respectively. As can be seen from the figures, the maximum stress and minimum factor of safety both occur at the point where the beam connects to the fixed point. This is expected for a cantilever beam.

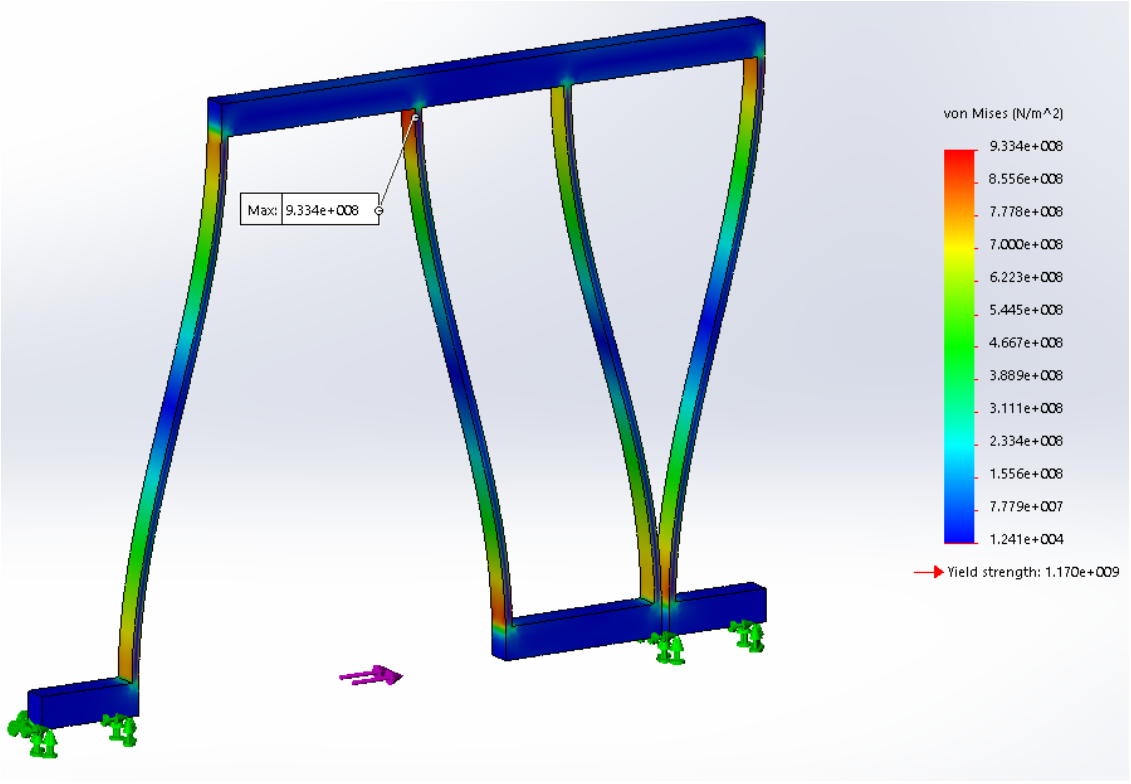

Figure 14: Stress Plot of Final Double Parallelogram Design

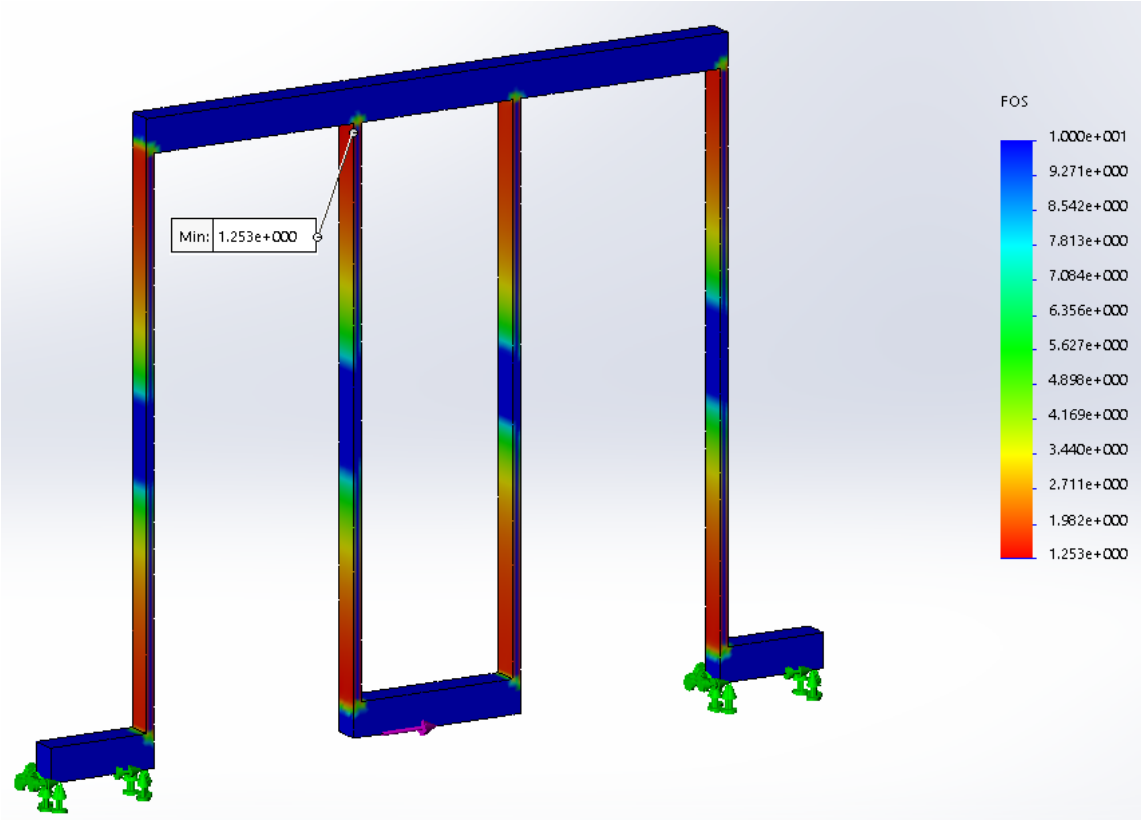

Figure 15: Factor of Safety Plot of Final Double Parallelogram Design

3.3 Vertical Stiffness (k_z) Design Analysis

From the overall design requirements listed in Table 1, the goal for the mechanism stiffness in the vertical direction was 0.005 N/mm. This stiffness value was predetermined since a very low stiffness value would increase the mechanism's ability to self-adapt to and more effectively grasp the surface of rock formations. In order to achieve this low stiffness value, the mechanism shown in Figure 9 was designed to have slider joints in the vertical direction with stainless steel extension springs attached to the mechanism at one end and looped around a peg in the center. A simplified diagram of this extension spring assembly is shown in Figure 16.

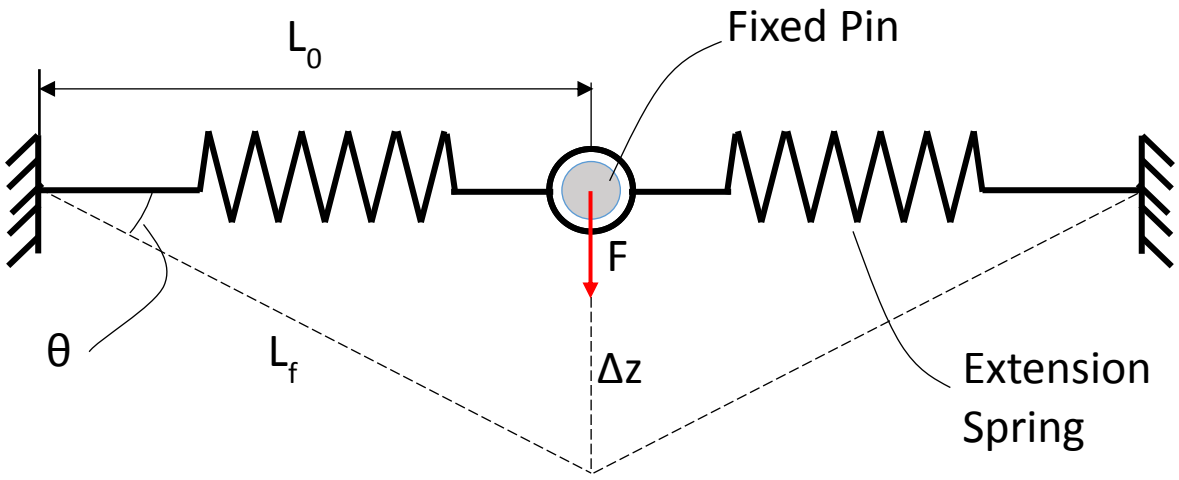

Figure 16: Extension Spring Force Diagram

In Figure 16, L_0 is the original, undeflected length of the spring, L_f is the final length of the spring after its deflection, and Δz simulates the vertical travel distance of the mechanism as the springs move through an angle θ. The goal for this analysis is to find the effective vertical stiffness (k_z) of the two springs during deflection in terms of the stiffness of the spring (k_s). From an analysis of Figure 16, equation (20) is derived for the parameters shown in the model.

$$L_f = \frac{L_0}{cos\theta} \tag{20}$$

The change in length of the extension spring can then be found in equation (21) as:

$$\Delta L = L_f - L_0 = \frac{L_0}{cos\theta} - L_0 \quad \rightarrow \quad \Delta L = L_0\left(\frac{1}{cos\theta} - 1\right) \tag{21}$$

Using Hooke's Law, the equation for the force of the spring can be written and substituted in equation (21) to simplify as:

$$F_s = k_s \Delta L \quad \rightarrow \quad F_s = k_s * L_0\left(\frac{1}{cos\theta} - 1\right) \tag{22}$$

Now, the force on the spring in the vertical direction can be expressed in terms of the force applied to the spring. Since the above analysis was performed on only one spring, but this design uses two springs in parallel, the equation is multiplied by two to get the correct equilibrium equation. This is shown in equation (23).

$$F_z = 2 * F_s sin\theta \tag{23}$$

Equation (23) can be further simplified by substituting the result from equation (22) for F_s, resulting in:

$$F_z = 2 * k_s * L_0\left(\frac{1}{cos\theta} - 1\right) * sin\theta \tag{24}$$

The vertical stiffness value for the mechanism is now found by using Hooke's Law in the vertical direction to set up equation (25).

$$k_z = \frac{F_z}{\Delta z} \tag{25}$$

A tangent relation is used to find Δz from Figure 14:

$$tan\theta = \frac{\Delta z}{L_0} \quad \rightarrow \quad \Delta z = L_0 tan\theta \tag{26}$$

Substituting equations (24) and (26) into equation (25) and simplifying yields:

$$k_z = \frac{2 * k_s * L_0 \left(\frac{1}{cos\theta} - 1\right) * sin\theta}{L_0 tan\theta} \quad \rightarrow \quad k_z = 2 * k_s * (1 - cos\theta) \tag{27}$$

Equation (27) shows the relationship between the vertical stiffness of the mechanism and the stiffness of the extension spring. What is unique about this relationship is that when the springs are in their natural position at θ=0°, the vertical stiffness of the mechanism is 0 N/mm. This is a desirable characteristic for the mechanism because it enables the spine to more easily adapt to the surface of the rock and find a suitable location to grasp. As the theta value increases, so does the vertical stiffness. This helps the mechanism return back to its starting position without the aid of gravity while in a microgravity environment.

Equation (27) can also be written in terms of the original length of the spring L_0 and vertical deflection Δz instead of the deflection angle θ. This is done by making a simple tangent substitution and is shown in equation (28).

$$k_z = 2 * k_s * \left(1 - \cos\left(tan^{-1}\left(\frac{\Delta z}{L_0}\right)\right)\right) \tag{28}$$

Since spring manufacturers specify standard sized springs with a given initial length and spring stiffness, it was then possible to plot the vertical stiffness (k_z) of the mechanism at a certain mechanism deflection (Δz). The Wolfram Mathematica Code in Appendix A titled "Extension Spring Calculations" shows various plots of the vertical stiffness versus mechanism deflection for springs of different length, stiffness, and wire diameter. Only springs that had an outside wire diameter of 1.6 mm were evaluated because the overall thickness of the part is 1.5875 mm, making this outside spring diameter slightly larger but still an acceptable size for the mechanism to function properly.

After an evaluation of all the stiffness versus deflection curves for the different springs, a spring was chosen to use in the prototype that best met the design requirements. This stainless steel spring had parameters of a 1.6 mm outside diameter, 0.228 mm wire diameter, length of 19.049 mm, and spring stiffness of 0.12 N/mm. Using two of these extension springs in the design shown in Figure 9, the overall mechanism stiffness was plotted as a function of the vertical deflection and is shown in Figure 17.

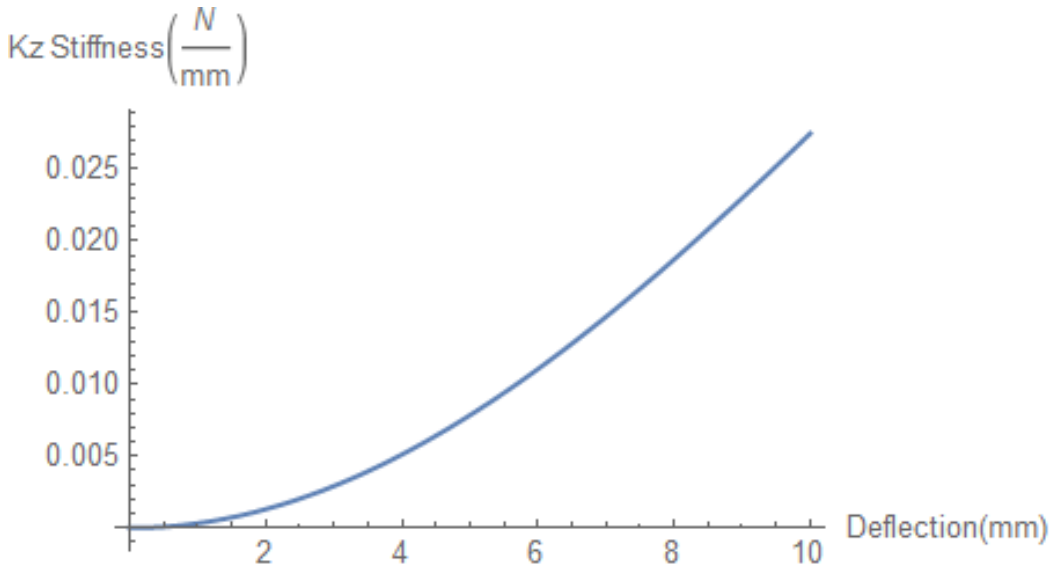

Figure 17: Mechanism Vertical Stiffness versus Deflection

The graph in Figure 17 shows that the design goal of k_z=0.005 N/mm is achieved at a vertical deflection of around 4 mm. The graph also shows almost a four times increase in stiffness to 0.020 N/mm for doubling the displacement to an 8 mm travel distance. These mechanism properties are ideal in two ways. The mechanism has a very low stiffness at a small displacement which increases the adaptability to differently shaped rock surfaces. Second, the non-linear shape of the curve increases the stiffness at higher displacements. This provides a restoring force to drive the spine into the rock surface to provide a stronger attachment.

Research continues to be performed to determine the optimal deflection at which the stiffness of 0.005 N/mm should occur and how the stiffness should increase for the mechanism to self-adapt to rock surfaces easier. This will be determined by prototyping and testing various spring sizes to see which ones perform better in terms of both self-adapting to the rock surface and providing a sturdy grip for supporting high loads. The final design in Figure 9 can also easily accommodate different length springs by simply changing the length of the mechanism spring hook with respect to the fixed pin in the center. This enables testing of different length springs without changing the entire design.

Chapter 4: Conclusion

The purpose of this research project was to develop, prototype, and optimize a new concept design for a compliant mechanism microspine gripper capable of achieving higher load sharing capabilities in a reduced overall size.

4.1 Contributions

Increased interest has been placed on furthering space exploration in recent years. Navigating effectively on planetary surfaces in microgravity and extreme terrain environments has proven a difficult challenge for current robots. Since most conventional locomotion techniques used on Earth are not ideal or practical for use in space, there was a need to develop a non-traditional method of anchoring and mobility for rovers in space. These limitations motivated the design and development of a new compliant gripping mechanism.

This compliant mechanism device utilizes a titanium material to provide high strength while still achieving the flexibility of an elastic material. This mechanism has a significant

advantage over the capabilities of previous devices by decoupling its vertical and horizontal motions, allowing the mechanism to have a different stiffness in these two directions which increases its ability to conform to rock surfaces easier while still being able to support high loads. The planar 2D design also allows multiple mechanisms to be placed adjacent to one another for compactness and minimal space. Arraying many microspines will allow the device to support even larger loads. This new mechanism design yields a cost effective and simple means for incorporation into a robotic arm to allow for a new way for robots to explore in space environments.

4.2 Future Work

In addition to studying the force versus deflection characteristics of the current design, it will be important to study these parameters in a more realistic setting and mechanism movement. The mechanism will need to be tested on an actual rock surface to see how well it can conform to varying surfaces and see if it is still able to support high loads. Another important design characteristic that will need to be tested is arraying a large quantity of the mechanisms next to one another to see how they interact. This will help to determine a more realistic loading pattern and determine if there are any interaction issues between adjacent microspines during testing. Testing many microspines in an array could involve designing a further compact carriage and utilizing additional electrical components to obtain a more realistic motion of the mechanism.

Another possible area that can be explored is looking into the actual interaction between the microspine and the rock surface it is gripping to try to enhance the mechanism. This interaction was not studied in this research due to its complex nature and difficulty in modeling. However, future work could be performed to determine the size characteristics of the spine that

reduce the overall stresses in the design and allow for a larger load-supporting capacity before failure.

4.3 Summary

In this research, a compliant mechanism microspine gripper was created as an alternative and unique method for rover anchoring and mobility in space applications. This mechanism has advantages over current devices since it is made fully of space-grade materials, its motion in the horizontal and vertical directions are highly independent of one another, many mechanisms can be compactly arrayed next to each other, and the mechanism is easy to manufacture at a low cost. The design of the mechanism relied heavily upon iteratively prototyping and testing multiple designs for their feasibility. An analysis was conducted to determine a general indication of the stiffnesses the mechanism was able to achieve and be used as a model to later optimize design parameters to decrease the overall size. SolidWorks FEA was also used to quantify the gripping force of the mechanism and determine the stresses and factor of safety in the design. This research will be valuable in pioneering alternative ways of anchoring and mobility for rovers to more safely and efficiently explore further regions in space.

Appendix A – Mathematica Code

Double Cantilever Beam Optimization

```
Clear["Global`*"]
```

Background Design Equations

```
Fsol = Solve[Δmax == F * L^3 / (12 * EE * I1), F]
(*Max deflection for a beam with one end fixed and the other end guided*)
Δmaxvalue = 6; (*Max deflection of inside beam part (in mm)*)
```

$$\left\{\left\{F \to \frac{12\ EE\ I1\ \Delta max}{L^3}\right\}\right\}$$

```
Mmax = F * L / 2 /. Fsol
```

$$\left\{\frac{6\ EE\ I1\ \Delta max}{L^2}\right\}$$

```
c = tmax / 2;
σmax = Mmax * c / I1 (*Maximum stress within the vertical beam segment*)
```

$$\left\{\frac{3\ EE\ tmax\ \Delta max}{L^2}\right\}$$

Castigliano's Theorem Derivation

```
moment[x_] := F * x
M = moment[x] (*Defining the moment as a function of x*)
```

$$F\ x$$

```
moi[x_] := 1/12 * b * (thickness[x])^3
I1 = moi[x] (*Defining the Moment of Intertia as a function of x*)
```

$$\frac{1}{12}\ b\ thickness[x]^3$$

```
Uinternal = ∫_0^(L/2) M^2/(2 * EE * I1) dx
```

$$\int_0^{\frac{L}{2}} \frac{6\,F^2\,x^2}{b\,EE\,thickness[x]^3}\,dx$$

```
Δhalfbeam = D[Uinternal, F]
 (*Taking the partial derivative of energy to find deflection of the half-beam model*)
```

$$\int_0^{\frac{L}{2}} \frac{12\,F\,x^2}{b\,EE\,thickness[x]^3}\,dx$$

Test with random variables:

```
Force1 = Input["Please input the Force on the bottom microspine in Newtons"];

F = Force1 / 2;

L = Input["Please input the vertical length of the beam in millimeters"];

thickness[x_] = 0.5; (*0.5*)

KnownParametersTi = {b → 1.5875, EE → 1.14 * 10^5, Sy → 1170};

HalfBeamDeflection =
 Δhalfbeam /. KnownParametersTi (*Half-Beam deflection given in millimeters*)
0.606404

Δmechanismoverall = HalfBeamDeflection * 4 (*Overall Deflection of mechanism*)
2.42562

kxfound = Force1 / (HalfBeamDeflection * 2)
0.824533

kxoverall1 = kxfound / 2
0.412266
```

Discretization Calculations

```
Clear["Global`*"]

Force1 = 6;

F = Force1 / 2;

b = 1.5875; EE = 1.14 * 10^5;

DeltaX = 12 ; (*Defining the max travel distance in x-direction*)

Deltabeamhalf = DeltaX / 4;
```

```
Sy = 1170; (*Yield Strength of Ti in N/mm^2*)

n = 100; (*Arbitrarily picking the number of discretized segments*)

ThicknessofI[i_, A_, B_, C_] := A * i^(1/2) + B * i + C

(* L= ( 2*n^3*b*EE / (3*kxgoal*Sum_{i=1}^{n} i^2/(ThicknessofI[i])^3) )^(1/3) *)

(*Calculated overall beam length in terms of a thickness function*)

ObjectiveL[A_, B_, C_] := ( 2 * n^3 * b * EE * Deltabeamhalf / (3 * F * Sum_{i=1}^{n} i^2/(ThicknessofI[i,A,B,C])^3) )^(1/3);

ConstMinThickness[A_, B_, C_] := Min[Table[ThicknessofI[i, A, B, C], {i, 1, n}]]

MaxStressOverall[A_, B_, C_] :=
 Max[Table[3 * EE * ThicknessofI[i, A, B, C] * (DeltaX/2) / ObjectiveL[A, B, C]^2, {i, 1, n}]]

ObjectiveL[0, 0, 0.5]
35.4561
```

Design Optimization

```
kxgoal = 0.5; (*Overall Kx stiffness goal*)

minThickness = 0.375;

minFOS = 1.25;

platedepth = 1.5875; (*1/16 in = 1.5875 mm *)

Sy = 1170;

StressMaxAllowed = Sy / minFOS
936.

sol = FindMinimum[
  {ObjectiveL[A, B, CC], A ≥ 0 && B ≥ 0 && ConstMinThickness[A, B, CC] ≥ minThickness &&
    MaxStressOverall[A, B, CC] ≤ StressMaxAllowed}, {{A, 0}, {B, 0}, {CC, minThickness}}]
{30.9158, {A → 1.80131 × 10^-11, B → 5.86338 × 10^-13, CC → 0.435974}}

ObjectiveL[0, 0, 0.5]
35.4561

ObjectiveL[0, 0, .45]
31.9104
```

```
ObjectiveL[-0.01, 0, 0.43597415447383236`]
ConstMinThickness[-0.01, 0, 0.43597415447383236`] ≥ minThickness &&
 MaxStressOverall[-0.01, 0, 0.43597415447383236`] ≤ StressMaxAllowed
```

```
24.7644
```

```
False
```

```
MaxStressOverall[-0.0001, 0, 0.43597415447383236`]
```

```
939.485
```

```
sol1 = sol[[1]];
```

```
sol2 = sol[[2]];
```

```
sol3 = sol2[[3]];
```

```
t = CC /. sol3;
```

```
thickfunc = ThicknessofI[x, A, B, CC] /. sol2
```

$$0.435974 + 1.80131 \times 10^{-11} \sqrt{x} + 5.86338 \times 10^{-13}\, x$$

```
Plot[thickfunc, {x, 0, n}, AxesLabel → {Discretized Segments, thickness [mm]}]
```

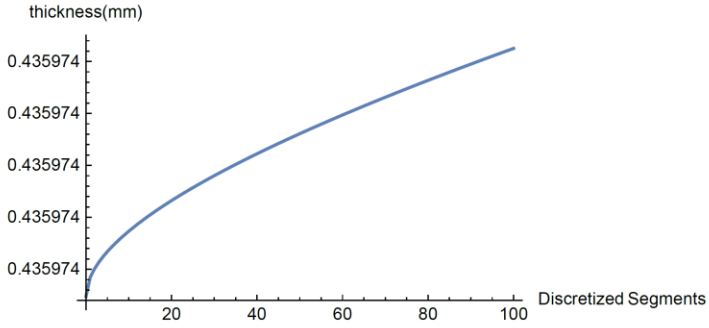

Design Equations

```
ClearAll[l1, l2, l3, t1, t2, t3, b, d3, d4, n, EE, Sy, Fz]
(*l1=length of initial horizontal spring*)
(*l2=length of spring from centerline to top or bottom*)
(*l3=length of final horizontal segment*)
(*t1=thickness of initial horizontal segment*)
(*t2=thickness of spring segments*)
(*t3=thickness of final horizontal segment*)
(*b=in-plane thickness*)
(*d3=horizontal length of one "n" segment*)
(*d4=length of beamgap*)
(*n=number of spring segments*)
(*EE=Elastic Modulus*)
(*Sy=Yield Strength*)
```

$$I1 = \frac{1}{12} * b * t1\text{^}3;\ I2 = \frac{1}{12} * b * t2\text{^}3;\ I3 = \frac{1}{12} * b * t3\text{^}3;\ (*\text{Defining moments of Inertia}*)$$

```
d3 = 2 * t2 + 2 * d4; (*Length of one segment*)
Ltotal = l1 + l3 + n * d3 ; (*Length of half spring element*)
Loverall = Ltotal * 2; (*Total Length of whole spring mirrored*)
```

$$kxeffective = \left(\frac{3 * EE * I2}{l2\text{^}3}\right) \Big/ (4 * n)$$

```
Fx = Simplify[kxeffective * 12] (*For 12mm travel distance*)
```

$$\frac{b\ EE\ t2^3}{16\ l2^3\ n}$$

$$\frac{3\ b\ EE\ t2^3}{4\ l2^3\ n}$$

$$\sigma maxtop = \frac{Fx * l2 * \left(\frac{t2}{2}\right)}{I2}$$

$$\sigma maxbottom = \frac{Fx * l2 * \left(\frac{t3}{2}\right)}{I2}$$

$$\frac{9\ EE\ t2}{2\ l2^2\ n}$$

$$\frac{9\ EE\ t3}{2\ l2^2\ n}$$

```
kzh1 = (3 * EE * I1 / l1^3); (*Initial horizontal beam*)
kzh2 = (3 * EE * I2 / (2 * n * d3)^3); (*Top and Bottom springs*)
kzh3 = (3 * EE * I3 / l3^3); (*Final horizontal beam*)
kzheffective = (1/kzh1 + 1/kzh2 + 1/kzh3)^-1 (*Effective horizontal spring constant*)
```

$$\frac{1}{\frac{4\,l1^3}{b\,EE\,t1^3}+\frac{32\,n^3\,(2\,d4+2\,t2)^3}{b\,EE\,t2^3}+\frac{4\,l3^3}{b\,EE\,t3^3}}$$

```
deltatopleft = Sum[Fz * l2 / EE * I2 * (Ltotal - (i - 1) * d3)^2, {i, 1, n}];
deltatopright = Sum[Fz * l2 / EE * I2 * (Ltotal - i * (d4 + t2) - (i - 1) * (d4 + t2))^2, {i, 1, n}];
deltabottomleft = Sum[Fz * l2 / EE * I2 * (Ltotal - i * (d4 + t2) - (i - 1) * (d4 + t2))^2, {i, 1, n}];
deltabottomright = Sum[Fz * l2 / EE * I2 * (Ltotal - (n * d3))^2, {i, 1, n}];

totaldelta = deltatopleft + deltatopright + deltabottomleft + deltabottomright;
kzveffective = Fz / totaldelta;

kzeffective = Simplify[(1/kzheffective + 1/kzveffective)^-1]
 (*Spring constant for force in Fz*)
```

$$\begin{aligned}&(b\,EE\,t1^3\,t2^3\,t3^3)\,/\\&\big(4\,(l3^3\,t1^3\,t2^3+12\,l2\,l3^2\,n\,t1^3\,t3^3+6\,l2\,l3\,n\,t1^3\,(d4+4\,l1+3\,d4\,n+t2+3\,n\,t2)\,t3^3+\\&\quad(12\,l1^2\,l2\,n\,t1^3+64\,d4^3\,n^3\,t1^3+6\,l1\,l2\,n\,(1+3\,n)\,t1^3\,t2+l1^3\,t2^3+\\&\quad\quad6\,d4^2\,n^2\,t1^3\,(l2+2\,l2\,n+32\,n\,t2)+2\,n^2\,t1^3\,t2^2\,(3\,l2+6\,l2\,n+32\,n\,t2)+\\&\quad\quad6\,d4\,n\,t1^3\,(l1\,(l2+3\,l2\,n)+2\,n\,t2\,(l2+2\,l2\,n+16\,n\,t2)))\,t3^3)\big)\end{aligned}$$

```
kzactual = kzeffective * 2; (*kz for the whole top spring element*)
```

Design Solutions

```
platedepth = 1.5875; (*1/16in = 1.5875 mm*)
beamgap = 1.2;
KnownParameters = {l1 → 1.10, l2 → 12, l3 → 5, t1 → .375, t2 → .375, t3 → .375,
   b → platedepth, d4 → beamgap, n → 10, EE → 1.14 * 10^5, Sy → 1170, Fz → 0.002};
(*Ti-13 heat treated with units of N/mm^2*)
```

```
kznumeric = kzactual /. KnownParameters
```

```
0.00534197
```

```
Lengthbeam = Loverall /. KnownParameters
```

```
75.2
```

```
Width = (n * d3) + (l1 - t2/2) + (l3 + t2/2);
Height = 2 * l2;
AreaSize = Width * Height
```

$$2\,l2\,(l1 + l3 + n\,(2\,d4 + 2\,t2))$$

Design Optimization

```
kzgoal = 0.005;
minFOS = 1.25;
minThickness = 0.375;
platedepth = 1.5875; (*1/16in = 1.5875 mm*)
beamgap = 1;
KnownParametersTi = {b → platedepth, EE → 1.14 * 10^5, Sy → 1170};
(*Ti-13 heat treated with units of N/mm^2*)
```

```
AreaSize1 = AreaSize /. KnownParametersTi
kzeffective1 = kzactual /. KnownParametersTi;
```

$$2\,l2\,(l1 + l3 + n\,(2\,d4 + 2\,t2))$$

```
DesignSolution = FindMinimum[
  {Abs[Loverall /. KnownParametersTi], (kzactual /. KnownParametersTi) == kzgoal &&
    2 ≥ t1 ≥ minThickness && 2 ≥ t2 ≥ minThickness && 2 ≥ t3 ≥ minThickness &&
    n ≥ 1 && ((σmaxtop /. KnownParametersTi) ≤ ((Sy /. KnownParametersTi)/minFOS)) &&
    ((σmaxbottom /. KnownParametersTi) ≤ ((Sy /. KnownParametersTi)/minFOS)) &&
    (Loverall /. KnownParametersTi) ≤ 70 && l1 ≥ 1 && 15 ≥ l2 ≥ 1 && l3 ≥ 2 && d4 ≥ 0.5},
  {{n, 3}, {t1, minThickness}, {t2, minThickness}, {t3, minThickness},
   {l1, 1}, {l2, 3}, {l3, 2}, {d4, .5}}]
```

```
{61.6913,
 {n → 15.9118, t1 → 1.14052, t2 → 0.375, t3 → 0.375071, l1 → 1., l2 → 15., l3 → 2., d4 → 0.5}}
```

Extension Spring Calculations

General Calculations

```
Kz = 2 * Ks * (1 - Cos[ArcTan[Δz / L0]]) (*Vertical Spring Stiffness in N/mm*)
```

$$2\,Ks\left(1-\frac{1}{\sqrt{1+\frac{\Delta z^2}{L0^2}}}\right)$$

Lee Springs Company

Lee Spring 1.6 mm OD, 0.177 mm WD, L=6.350 mm, KS=0.14 N/mm, SS, Part #: EI 007A 01 S

```
Plot[Kz /. {L0 → 6.350, Ks → 0.14 (*N/mm*)},
 {Δz, 0, 10}, AxesLabel → {Deflection [mm], Stiffness [N / mm]}]
```

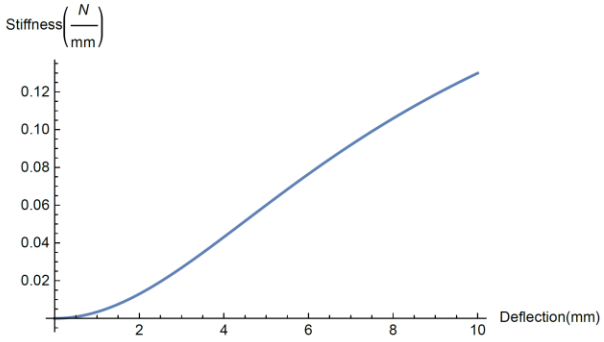

Lee Spring 1.6 mm OD, 0.279 mm WD, L=11.125 mm, KS=0.70 N/mm, SS, Part #: EI 011A 04 S

```
Plot[Kz /. {L0 → 11.125, Ks → 0.70 (*N/mm*)},
 {Δz, 0, 10}, AxesLabel → {Deflection [mm], Stiffness [N / mm]}]
```

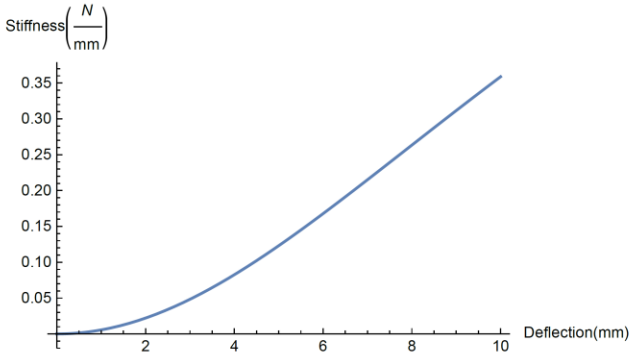

Lee Spring 1.6 mm OD, 0.177 mm WD, L=12.7 mm, KS=0.05 N/mm, SS, Part #: EI 007A 05 S

```
Plot[Kz /. {L0 → 12.7, Ks → 0.05 (*N/mm*)},
 {Δz, 0, 10}, AxesLabel → {Deflection [mm], Stiffness [N / mm]}]
```

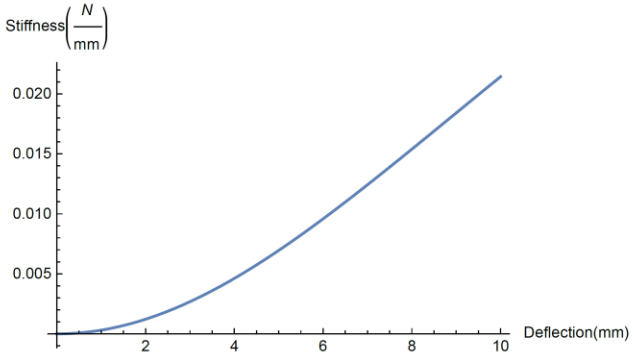

Lee Spring 1.6 mm OD, 0.228 mm WD, L=19.049 mm, KS=0.12 N/mm, SS, Part #: EI 009A 07 S

```
Plot[Kz /. {L0 → 19.049, Ks → 0.12 (*N/mm*)},
 {Δz, 0, 10}, AxesLabel → {Deflection [mm], "Kz" Stiffness [N / mm]}]
```

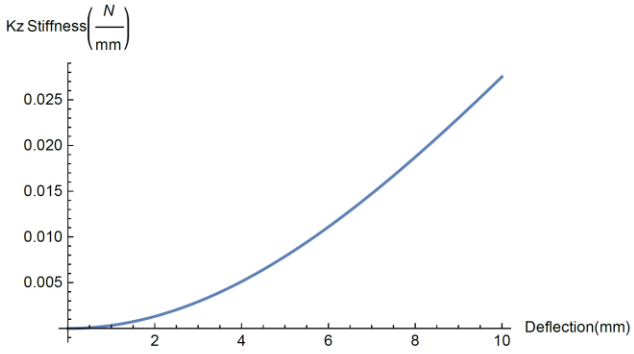

Lee Spring 1.6 mm OD, 0.228 mm WD, L=22.224 mm, Ks=0.10 N/mm, SS, Part #: EI 009A 08 S

```
Plot[Kz /. {L0 → 22.224, Ks → 0.10 (*N/mm*)},
 {Δz, 0, 10}, AxesLabel → {Deflection [mm], Stiffness [N / mm]}]
```

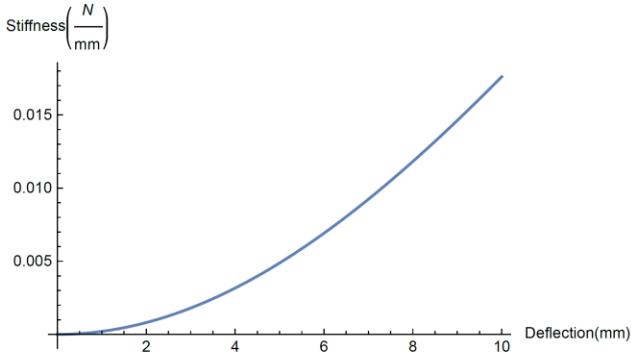

Lee Spring 1.6 mm OD, 0.203 mm WD, L=22.224 mm, Ks=0.05 N/mm, SS, Part #: EI 008A 08 S

```
Plot[Kz /. {L0 → 22.224, Ks → 0.05 (*N/mm*)},
 {Δz, 0, 10}, AxesLabel → {Deflection [mm], Stiffness [N / mm]}]
```

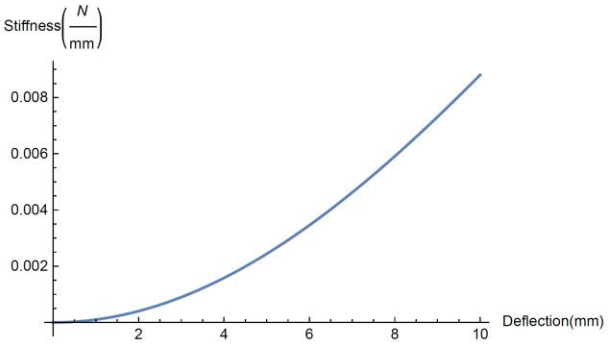

Century Springs

Murphy and Read Spring Company

Determining Ks and Lo from specified Kz and Δz values

```
Clear["Global`*"]
```

```
Equation1 = Kz - (2 * Ks * (1 - Cos[ArcTan[Δz / L0]])) (*Solving Equation to set equal to 0*)
```

$$Kz - 2\,Ks\left(1 - \frac{1}{\sqrt{1 + \frac{\Delta z^2}{L0^2}}}\right)$$

```
subs1 = {Kz → 0.005, Δz → 3}
 (* Making a random substitution to specify Vertical Stiffness at a certain deflection*)
```

```
{Kz → 0.005, Δz → 3}
```

```
ListPlot[Table[{i, Ks /. FindRoot[Equation1 /. subs1 /. L0 → i, {Ks, 0.01}]}, {i, 5, 25}]]
```

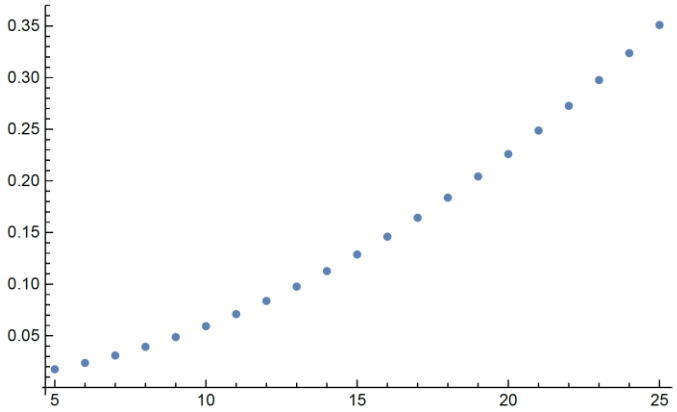

Appendix B – Final Design Diagram with Parameters

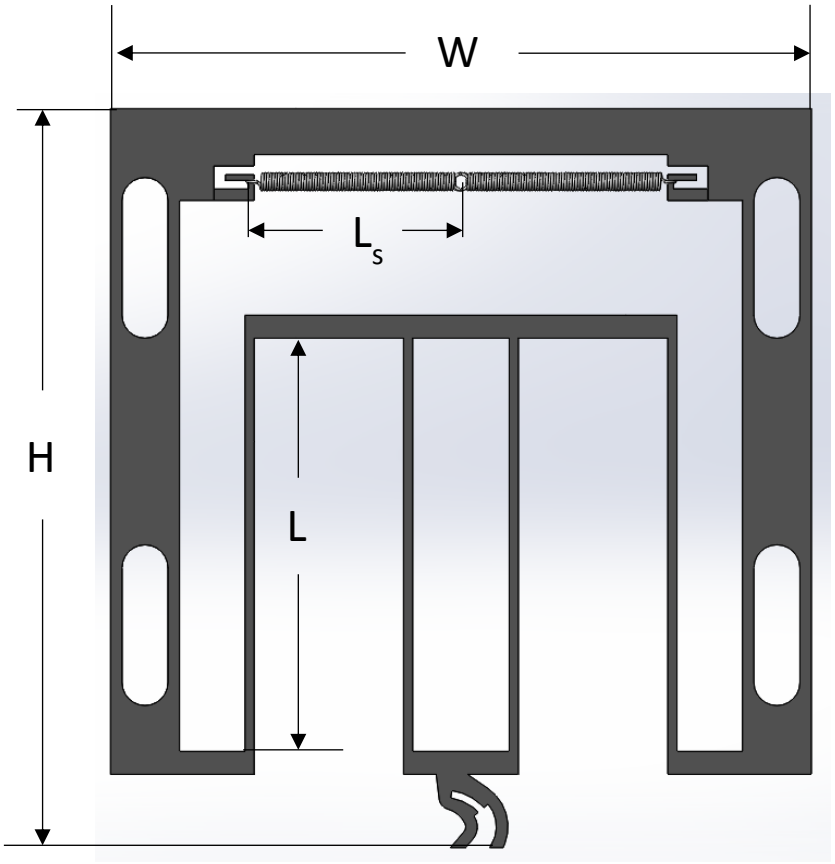

Parameter	Symbol	Value (mm)
Width	W	60.54
Height	H	60.98
Double Parallelogram Beam Lengths	L	32.6
Spring Length	L_s	19.05
Out-of-plane thickness	b	1.5875

References

Abell, P. et al., 2016. *The Asteroid Redirect Mission (ARM).* s.l., s.n.

Anon., 2015. *NASA Technology Roadmaps TA 4: Robotics and Autonomous Systems.* [Online] Available at: http://www.nasa.gov/sites/default/files/atoms/files/2015_nasa_technology_roadmaps_ta_4_robotics_and_autonomous_systems_final.pdf [Accessed October 2016].

Asbeck, A. T. & Cutkosky, M. R., 2012. Designing Compliant Spine Mechanisms for Climbing. *Journal of Mechanisms and Robotics.*

Asbeck, A. T. et al., 2006. Scaling Hard Vertical Surfaces with Compliant Microspine Arrays. *The International Journal of Robotics,* 25(12).

Autumn, K. et al., 2005. Robotics in scansorial environments. *Unmanned Ground Vehicle Technology VII,* Volume 5804.

Autumn, K. et al., 2006. Dynamics of geckos running vertically. *Journal of Experimental Biology,* pp. 260-272.

Cutkosky, M. R. & Kim, S., 2009. Design and fabrication of multi-material structures for bioinspired robots. *Biomimetics II: fabrication and applications,* 30 March.367(1894).

Hackett, J., 2016. *Robotic Comet Lander Philae Says Good-Bye.* [Online] Available at: https://www.scientificamerican.com/article/robotic-comet-lander-philae-says-good-bye/

Howell, L. L., 2001. *Compliant Mechanisms.* s.l.:John Wiley & Sons, Inc..

Kim, S., Asbeck, A. T., Cutkosky, M. R. & Provancher, W. R., 2005. Spinybot II: Climbing hard walls with compliant microspines. *Advanced Robotics.*

Koli, A. B., 2013. A generalized approach for compliant mechanism design using the synthesis with compliance method, with experimental validation. *Scholars' Mine.*

Merriam, E. G. et al., 2016. Microspine Gripping Mechanism for Asteroid Capture. *All Student Publications.*

Parness, A., 2011. *Anchoring foot mechanisms for sampling and mobility in microgravity.* s.l., s.n.

Parness, A., Frost, M., Thatte, N. & King, J. P., 2012. *Gravity-independent mobility and drilling on natural rock using microspines.* s.l., s.n.

Parness, A. et al., 2013. Gravity-independent Rock-climbing Robot and a Sample Acquisition Tool with Microspine Grippers. *Journal of Field Robotics,* 30(6).

Zacny, K. et al., 2008. Drilling Systems for Extraterrestrial Subsurface Exploration. *ASTROBIOLOGY,* 8(3).